



# PROJECT FINAL REPORT

**Grant Agreement number: ACP3-GA-2014-620327**

**Project acronym: HEXAFLY-INT**

**Project title: High-Speed Experimental Fly Vehicles - International**

**Funding Scheme: FP7:**

**Collaborative Project: Small or Medium-Scale Focused Research Project**
**Theme 7: TRANSPORT**

**Date of latest version of Annex I against which the assessment will be made:**

**Period covered: from 1st of April 2014 to 30th of September 2019**

**Scientific representative of the project's coordinator:**

**Name: Dr J. Steelant**

**Title: Senior Engineer**

**Organisation: European Space Agency – European Space Research and Technology Centre (ESA-ESTEC)**

**Tel: +31/71/565.5552**

**Fax: +31/71/565.5421**

**E-mail: Johan.Steelant@esa.int**

**Project website address: www.esa.int/techresources/hexafly_int**

# APPROVAL

| Title | Issue | Revision |
|---|---|---|
| HEXAFLY-INT: Final Activity Report | 1 | 0 |

| Author(s) | Date |
|---|---|
| J. Steelant (ESA),<br>A. Kallenbach (DLR),<br>A. Wagner (DLR),<br>J.-Y. Andro (ONERA),<br>S. di Benedetto (CIRA),<br>B. Saracoglu (VKI) | *30/09/2019* |

| Approved by | Date |
|---|---|
| J. Steelant (ESA) | 30/11/2019 |

# CHANGE LOG

| Reasons for change | Issue | Revision | Date |
|---|---|---|---|
| | | | |
| | | | |

# CHANGE RECORD

| Issue | Revision | | |
|---|---|---|---|
| **Content of change** | **Date** | **Pages** | **Paragraph(s)** |
| | | | |

# Table of contents

## List of Figures

## List of Tables



## Nomenclature

*Acronyms*

| | |
|---|---|
| ATLLAS | Aero-Thermal Loaded Material Investigations for High-Speed Vehicles |
| BL | Boundary Layer |
| BLT | Boundary Layer Transition |
| CFD | Computational Fluid Dynamics |
| EC | European Commission |
| EFTV | Experimental Flight Test Vehicle |
| ESM | Experiment Support Module |
| HEXAFLY | High-Speed Experimental Fly Vehicles |
| HXI | HEXAFLY-International |
| LAPCAT | Long-Term Advanced Propulsion Concepts and Technologies |

*Roman Symbols*

| | |
|---|---|
| T | temperature [K] |

*Greek Symbols*

| | |
|---|---|
| ρ | density [kg $m^{-3}$] |
| α | Angle of Attack |

*Superscripts and subscripts*

| | |
|---|---|
| ref | reference |
| 0 | Total values |

# 1 Final Publishable summary

## 1.1 An executive Summary

Civil high-speed passenger transport only makes sense when deployed for long-haul intercontinental flights. Consequently, the related development and deployment of such a high-speed vehicle will most likely demand an international approach. The internationally funded HEXAFLY-INT project is a first step in the direction of civil high-speed transportation along with an international development where flight-testing is the focal point.

The global aim is to flight test an experimental waverider-based vehicle concept above Mach 7 to verify its potential for a high cruise efficiency during a free-flight. In parallel, the concept will also be flight tested to prove the waverider concept is also able to take-off, to accelerate to subsonic speed and to land in an efficient and robust way.

The feasibility for a 3m long vehicle was demonstrated during the European precursor project HEXAFLY. Its realization is now being enabled on an international scale preparing the grounds for global cooperation in case of a future deployment of a high-speed cruiser. These flight opportunities will increase drastically the Technology Readiness Level of developments realized in previous high-speed EC projects such as ATLLAS I & II and LAPCAT I & II.

## 1.2 Project Context and Objectives

The overall objective of HEXAFLY is to create a generic high-speed platform enabling in-flight testing of several breakthrough technologies. To mature this idea, a scientific mission profile was worked out based upon a preliminary design of a high-speed flight test vehicle along with the identification of the most promising flight platform, e.g. sounding rocket. This combination would then offer the possibility to test out various technologies, grouped around the six major axes of HEXAFLY:

1. *High-Speed Vehicle Concepts* to assess the overall vehicle performance in terms of cruise-efficiency, range potential, aero-propulsive balance, aero-thermal-structural integration, etc...
2. *High-Speed Aerodynamics* to assess aerodynamic vehicle shapes with high L/D, aerodynamic manoeuvrability, stability, etc…
3. *High-Speed Propulsion* to evaluate the performances of high-speed propulsive devices such as intakes, air-breathing engines, nozzles including phenomena such as high-speed combustion, injection mixing processes, etc…
4. *High-Temperature Materials and Structures* to flight-test under realistic conditions high temperature lightweight materials, cooling concepts, reusability aspects…
5. *High-Speed Flight Control* requiring real-time testing of Guidance Navigation Control in combination with technologies on Health Monitoring Systems/ Fault Detection and Isolation
6. *High-Speed Environmental Impact* focusing on reduction techniques for sonic boom and sensitivities of high-altitude emissions of $H_20$, $CO_2$, NOx on the stratosphere.

Following this general HEXAFLY philosophy, a first project on international level was proposed, *HEXAFLY-INTernational,* with the auspices of the European Community (EC) together with 11 partners from Europe (ESA, AIRBUS, CIRA, DLR, ONERA, TET, TSD, GDL, Marotta, Univ. of Stuttgart, VKI ), 4 from the Russian Federation (TsAGI, CIAM, LII and MIPT) and 3 from Australia (Univ. Sydney, UNSW, USQ). The overall aim is to design, manufacture and flight test a high-speed vehicle, based on the configuration developed in previous EC co-funded projects ATLLAS I & II [1][2][3], LAPCAT I & II [4][5], and HEXAFLY [6][7]. Under HEXAFLY-INT, both a glider and a hydrogen-propelled variant of the high-speed vehicle are being considered, the former being developed by EC partners with international partners, the latter being developed only by the Russian partners. The flight experiment carried out by the Europeans, Russians and Australians, is focused on

- Elaborating a self-controlled glider demonstrating a high aerodynamic efficiency in combination with a high internal volume
- a positive aerodynamic balance at a cruise Mach number of 7 to 8 in a controlled way
- making optimal use of advanced high-temperature materials and/or structures
- the aerodynamic gliding performance from Mach 8 down to Mach 2
- including several breakthrough technologies on-board [10],
- validating methods and technologies deployed in hypersonic vehicles design [7][10][11][12][14].

Two distinctly different flight tests are considered. One at high-speed checking the cruise capability of a potential civil passenger hydrogen fuelled high-speed vehicle, another at low-speed to check its handling qualities during take-off and landing.

The Experimental Flight Test Vehicle (EFTV), for testing the cruise performance as a non-propelled glider at high-speed will be launched by a sounding rocket (the Brazilian VS50 launcher based upon an 12-ton solid rocket motor) in a suborbital trajectory having an apogee at about 100 km ().

After the release from the launcher, the EFTV will perform the first part of the descent docked to the Experimental Service Module (ESM), which controls the vehicle attitude. As soon as the EFTV features full aerodynamic control authority, it undocks from the ESM and pulls out from its descent to perform a hypersonic cruise at approximately Mach 7. In this experimental phase, the EFTV aims to demonstrate as a glider a high aerodynamic efficiency (L/D≥4), a positive aerodynamic balance at controlled cruise Mach numbers (7÷8) and an optimal use of advanced high-temperature materials and structures. The overall mission requirements are listed in Table 1.
The vehicle design, manufacturing, assembly and verification are the main drivers and challenges in this project in combination with a sounding rocket tuned for the mission. Both the glider and the propelled options of the HEXAFLY-INT high-speed vehicle are characterized from the aerodynamic and aerothermodynamic points of view.

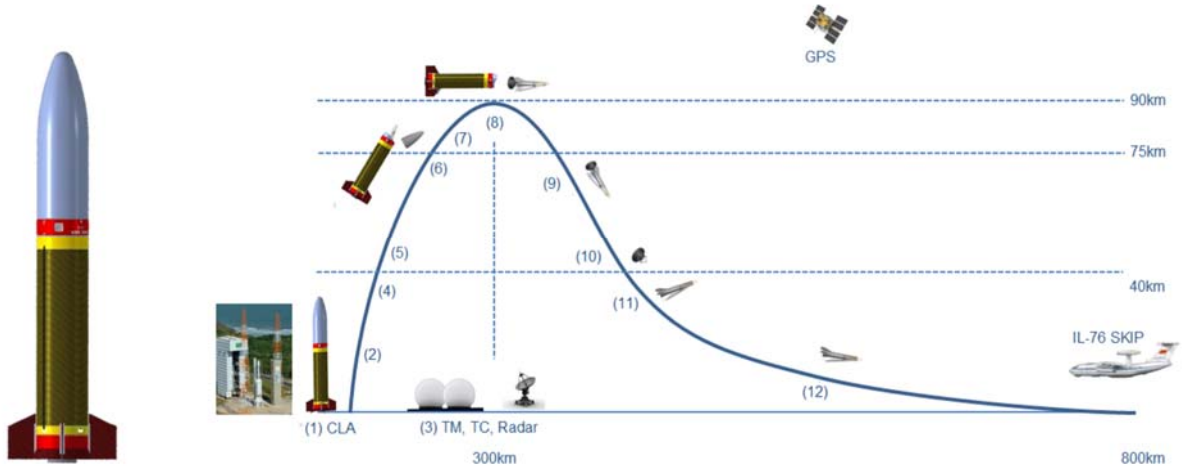


*Fig. 1 HEXAFLY-INT VS-50 launch vehicle (left) and overall mission profile (right).*

Table 1: Basic mission requirements for EFTV

| Requirement | Target Value | Min. Value | Max. Value | Comment |
|---|---|---|---|---|
| **Phase I: insertion into level flight: Mach number [-]** | 7.4 | 7 | 8 | Phase I: addressing aerodynamic balance after pull-out manoeuvre |
| **Phase II: Gliding Phase:**<br>**➔ Flight Mach number [-]** | 5 to 7.4 | 2 | 8 | Phase II: Mach number gradually dropping during gliding phase potentially including manoeuvres. |
| **Flight altitude [km]** | 30 | 27 | 33 | Optimal: level flight |
| **Flight path angle [º]**<br>**Phase I** | 0 (level) | 0 | 10 to 15 (TBD) | Accuracy: 0.1 (measured)<br>Accuracy: +/-5 (TBD) for insertion |
| **Test time (Phase II) [s]** | Max. possible | 150 | Till impact | Gliding Phase duration defined by aero-stability range |

Besides the high-speed flight experiment, an additional low-speed flight experiment will be performed to crosscheck the viability of the vehicle concept for later deployment as passengers' aircraft. It entails a flight experiment in the Danger Area 451 (Univ. of Sydney) to verify the take-off, cruising at a low subsonic speed and landing potential for the waverider-based vehicle and its related control authority.

The program was kicked off in April 2014 and will pass the CDR by end of 2018. The paper describes the status of the vehicle design along with the elements related to the flight preparation.

In parallel to the overall technical work to realize the different flights and experiments, a framework has been set up to ease the exchange of students of the involved universities among the different partners. This gives them a unique expertise of contributing to the different pieces of one of these flight experiments.

## 1.3 Main Science & Technology Results

### 1.3.1 Glider Concept

#### 1.3.1.1 General Layout of the Experimental Flight Test Vehicle (EFTV)

The EFTV, see Fig. 2, is a hypersonic glider of 3.29m length and having a span of about 1.23m. The EFTV has a two-dimensional nosetip with 2mm rounding and 2mm lateral fillet, while the wing is characterized by a 80° sweep angle and 14° negative dihedral angle, and 1mm rounded leading edge. As control surfaces, the vehicle is equipped by a couple of active ailerons (0.4m long and 0.32m wide), which can be deflected in symmetric and asymmetric way, and a couple of fixed vertical fins characterized by a 68.5° sweep angle and a 54° angle formed between the two fins in the transversal plane. The present aeroshape is the result of an evolution [10] that, following the suggestions by the continuous aero-heating assessment, has affected mainly the nosecap and forebody configuration, the wing (leading edge and fuselage intersection) and the aileron.

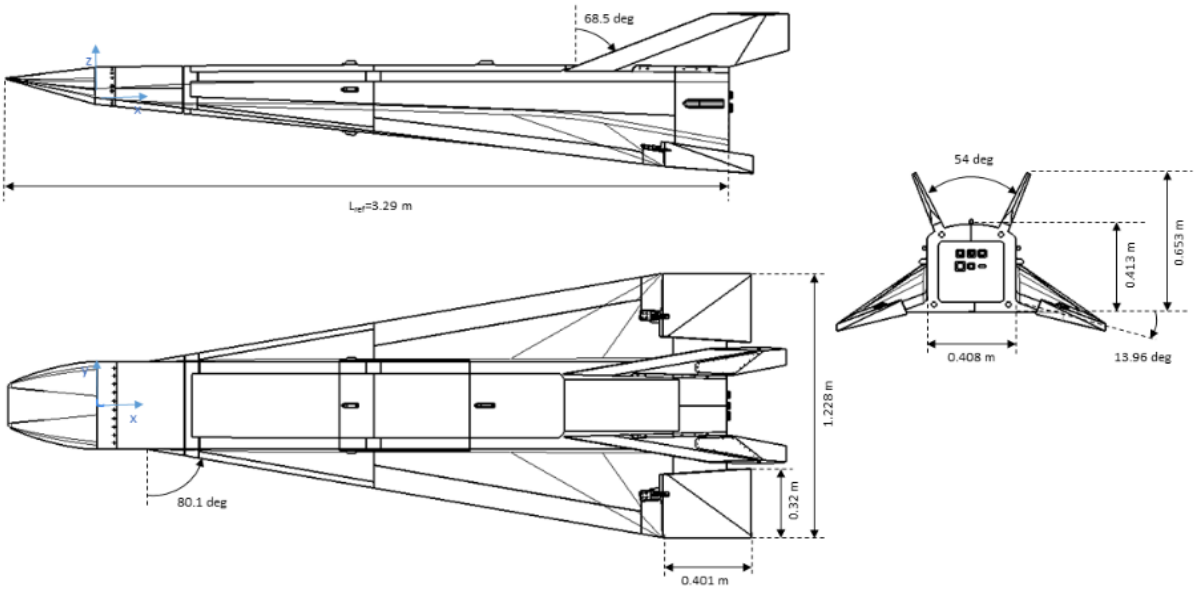


*Fig. 2: EFTV three-view drawing*

During ascent and first part of the re-entry phase after release from the rocket at the 90km apogee, the EFTV is coupled with the conically shaped Experiment Service Module ESM, which has a double function (*Fig. 3*). At first, it acts as the interface between the EFTV and the Launch Vehicle Service Module (LVSM) mounted on top of the S43 booster. Secondly, it will act as a weathercock aligning the EFTV to a certain attitude at 55km altitude from which it will then separate. It allows the EFTV to start its pull-out manoeuvre to bring the EFTV to a hypersonic levelled flight above Mach 7 and execute its overall mission objectives starting from a 30km altitude. A typical trajectory is given in Fig. 4. The ESM has also a Cold Gas System (CGS) on-board to assure attitude control in the exo-atmosphere once released from the LVSM.

As general material layout, the metallic structure of the EFTV, i.e. the fuselage, wing and vertical tail, is composed of titanium alloy, apart from the copper nose section. Wing leading edges and ailerons are in C/C-SiC (Fig. 5). The metallic exposed surface parts are thermally protected by high emissivity or $ZrO_2$ coatings. This material layout is compliant with the aerothermal loading conditions expected for the glider.

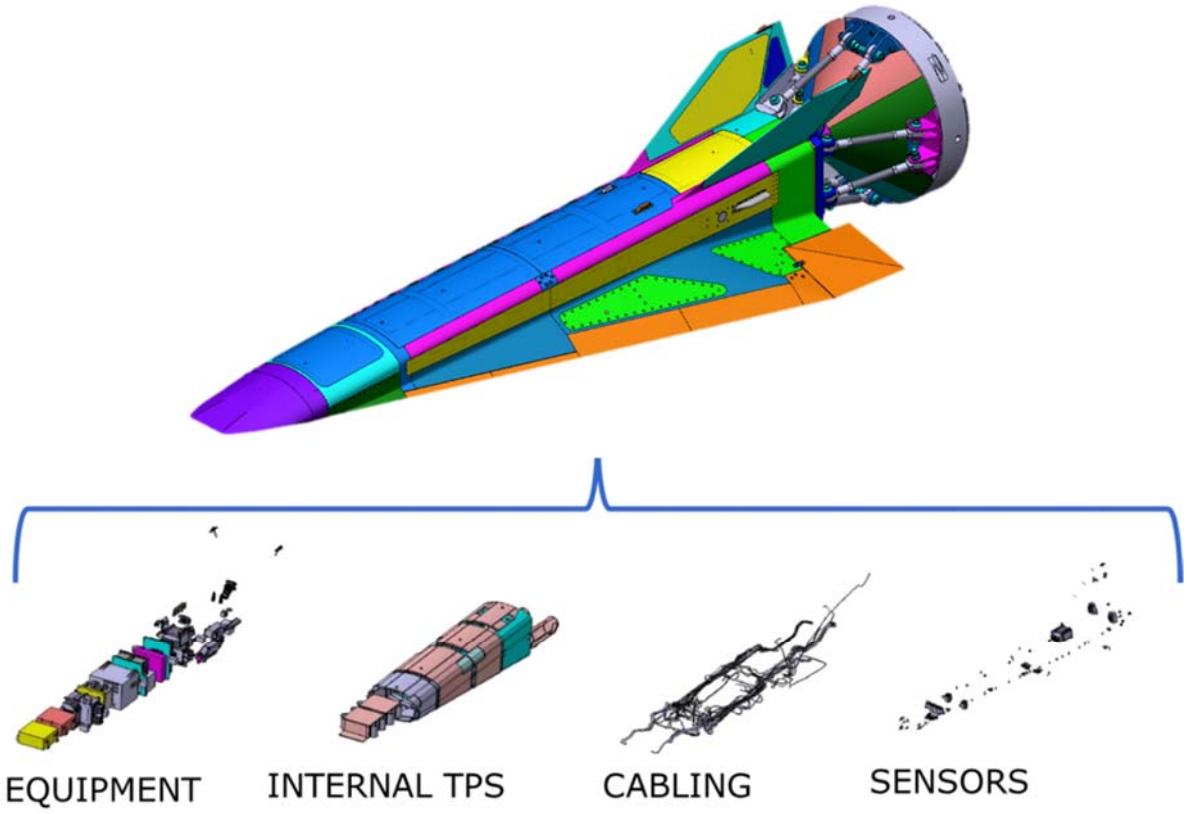


*Fig. 3: The EFTV glider with ESM.*

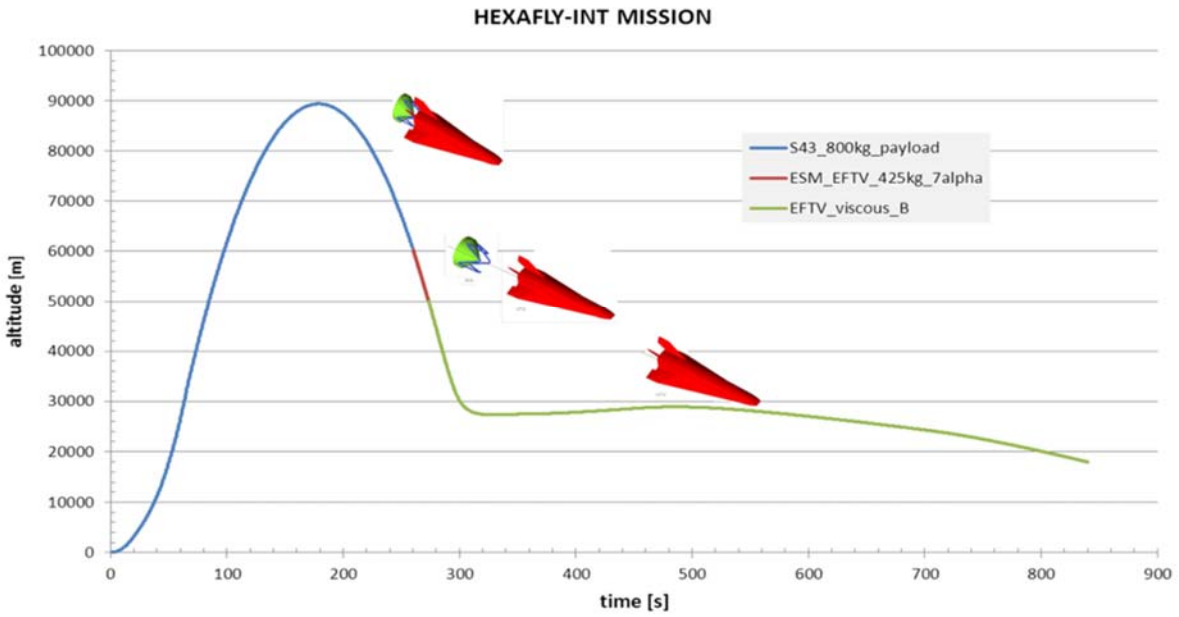


*Fig. 4: Altitude time history*

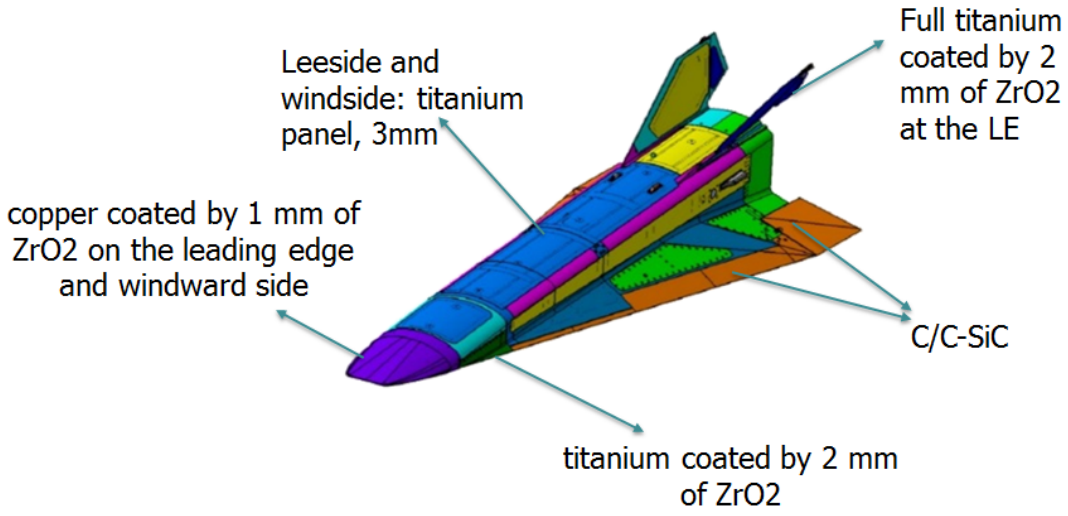


*Fig. 5: Final EFTV TPS Configuration: high emissivity painting on the EFTV metallic surfaces, even on coating*

The EFTV will be equipped with an avionic system composed of an inertial measurement unit, a GPS, two servo-actuators for the ailerons, and a flight control computer, which will ensure the on-board mission management. The vehicle will also be equipped with an in–flight measurement system acquiring pressure, temperature and acceleration data sensors for the sake of post flight analysis and simulation tools validation. The on-board avionics will also include a downlink telemetry system (i.e. with antennas) which will transmit all mission data to the Ground Control Station at the launch site. The overall layout of the EFTV vehicle is shown in Fig. 6.

In Fig. 7, the exploded view of the fuselage sections and the major components are shown. The fuselage structure is mainly composed by milled frames, upper beams and panels. The assembly of the fuselage structure is realized by joining the upper beam frames and lower panels with fixed bolts. The upper panels are joined to the frames and upper beams by removable bolts in order to allow easy access to the equipment located inside the fuselage. The tail fuselage is composed by two shells and a rear panel. The upper part is joined with a bolted strap whereas the bottom part is joined with an overlap between the two shells by two fixed bolts. The rear panel is bolted with removable bolts allowing access to the internal part of fuselage. The tail fuselage shells also include the provision for the pyro bolts installation. Further details on the multi-disciplinary design issues and related analyses can be found in [21].

#### 1.3.1.2 Flight Control

The design of control laws have been carried out considering longitudinal and lateral-directional rotational dynamics separately (*Fig. 8*). According to EFTV nominal trajectory, Mach number, angle of attack and dynamic pressure assume values within some ranges. Therefore, the control gains are computed in a 3-dimensional envelope in which the trajectory is expected to be contained. Obviously, since the angle of attack is a controlled variable, the reference AoA (not the actual one) is used as a scheduling variable. Control law designs were carried out with the aim of optimizing performances while guaranteeing a prescribed level of stability also in presence of model uncertainties, sensor errors, etc.

Being launched from Alcântara in Brazil, Fig. 9 shows a typical trajectory of the launcher (yellow) and the EFTV (white). Due to launch range constraints and telemetry limitations, the EFTV needs to remain within 600km from the coastline to assure the on-board collection of the experimental data is entirely transmitted to a ground station. Apart from a pull-out manoeuvre and a gliding phase, a banking manoeuvre is carried out assuring the vehicle remains within the range of the ground station (see [20] for further details). To carry out these different manoeuvres, an actuation system needs to be designed to cope with these different loads.

| ITEM N° | P/N | DESCRIPTION | QYT | RESP |
|---|---|---|---|---|
| 1 | BPK-4.02.1 | BATTERY_BOX_(3_strings) | 1 | TSD |
| 2 | BPK-4.02.2 | BATTERY_BOX_(3_strings) | 1 | TSD |
| 3 | HXI-IFM-MS1 | DAQ EBX | 1 | DLR_Co |
| 4 | HXI-IFM-MS2 | DAQ EBX | 1 | DLR_Co |
| 5 | DLR-RB-MRB_E-Box_HXI_EFTV | EBX1 | 1 | DLR_Mo |
| 6 | PMS-4.02.1 | POWER MANAGEMENT SYS | 1 | TSD |
| 7 | ISP17A915PMI1050-00 | BOITIER_CONNECTEURS-D | 1 | ONERA |
| 8 | ISP17A915PMI1050-00 | BOITIER_CONNECTEURS-D | 1 | ONERA |
| 9 | MRB-1000974 | DMARS IMU | 1 | CIRA |
| 10 | FCC-4.01.1 | FLIGHT CONTROL COMPUTER | 1 | TSD |
| 11 | DLR-RB-MRB_GPS_Receiver_Phoenix | GPS RECEIVER | 1 | DLR_Mo |
| 12 | DLR-RB-MRB_Coupler_S-Band_HXI_EFTV | S-BAND COUPLER | 2 | DLR_Mo |
| 13 | DLR-RB-MRB_Intus_S2460_TM | TM SENDER | 2 | DLR_Mo |
| 14 | DLR-RB-MRB_Intus_S2460_TV | TV SENDER | 2 | DLR_Mo |
| 15 | DLR-RB-MRB_Intus_UHF_E450 | TC RECEIVER | 2 | DLR_Mo |
| 16 | DLR-RB-MRB_Coupler_TC_HXI_EFTV | TC COUPLER | 1 | DLR_Mo |
| 17 | DAQ-MS2 | DAQ | 1 | DLR_Co |
| 18 | UNSW-EBOX-ASSEMBLY_ASM | EBOX | 1 | UNSW |
| 19 | UNSW_HXI_02_001 | MONOCHROME-CAMERA | 1 | UNSW |
| 20 | UNSW_HXI_03_001 | MONOCHROME-CAMERA | 1 | UNSW |
| 21 | UNSW_HXI_04_001 | LWIR_SWBLI_CAMERA | 1 | UNSW |
| 22 | UNSW_HXI_05_001 | LWIR_TRANSITION_CAMERA | 1 | UNSW |

| ITEM N° | P/N | DESCRIPTION | QYT | RESP |
|---|---|---|---|---|
| 23 | UNSW_HXI_06_001 | HXI_UV_LED_LAYOUT | 2 | UNSW |
| 24 | DLR-RB-MRB_GPS_Ant_HT_HXI_EFTV | GPS ANTENNA VF | 1 | DLR_Mo |
| 25 | DLR-RB-MRB_GPS_Ant_HT | GPS ANTENNA FUSELAGE | 1 | DLR_Mo |
| 26 | DLR-RB-MBR_S-Band_Ant_HT | S BAND ANTENNA FUSELAGE | 1 | DLR_Mo |
| 27 | DLR-RB-MBR_S-Band_Ant_HT_HXI_EFTV | S BAND ANTENNA VF | 1 | DLR_Mo |
| 28 | MODEL_OPTICAL | MODEL_OPTICAL | 1 | DLR_Co |
| 29 | IR MOUNTING | IR MOUNTING | 1 | DLR_Co |
| 30 | REARCAM | REARCAM | 1 | DLR_Co |
| 31 | DLR-RB-MRB_TC_Ant | TC Antenna | 2 | DLR_Mo |
| 32 | DLR-RB-MRB_TC_Ant_Cover | TC Antenna Cover | 2 | DLR_Mo |
| 33 | DLR-RB-MRB_GPS_Pre-Amplifier | GPS_Pre-Amplifier | 1 | DLR_Mo |
| 34 | 9151000 | IPS ACTUATOR | 2 | ONERA |
| 35 | DAQ-BOB0 | DAQ BREAK BOX | 1 | DLR_Co |
| 36 | DAQ-BOB1 | DAQ BREAK BOX | 1 | DLR_Co |
| 37 | HXI-IFM-BOB2A | DAQ BREAK BOX | 1 | DLR_Co |
| 38 | HXI-IFM-BOB2B | DAQ BREAK BOX | 1 | DLR_Co |
| 39 | DAQ-BOB3 | DAQ BREAK BOX | 2 | DLR_Co |
| 40 | DAQ-BOB4 | DAQ BREAK BOX | 1 | DLR_Co |
| 41 | DAQ-BOB5A | DAQ BREAK BOX | 1 | DLR_Co |
| 42 | DAQ-BOB5B | DAQ BREAK BOX | 1 | DLR_Co |
| 43 | MRB-1000777_NOVATEL_GNSS | GPS | 1 | DLR_Mo |

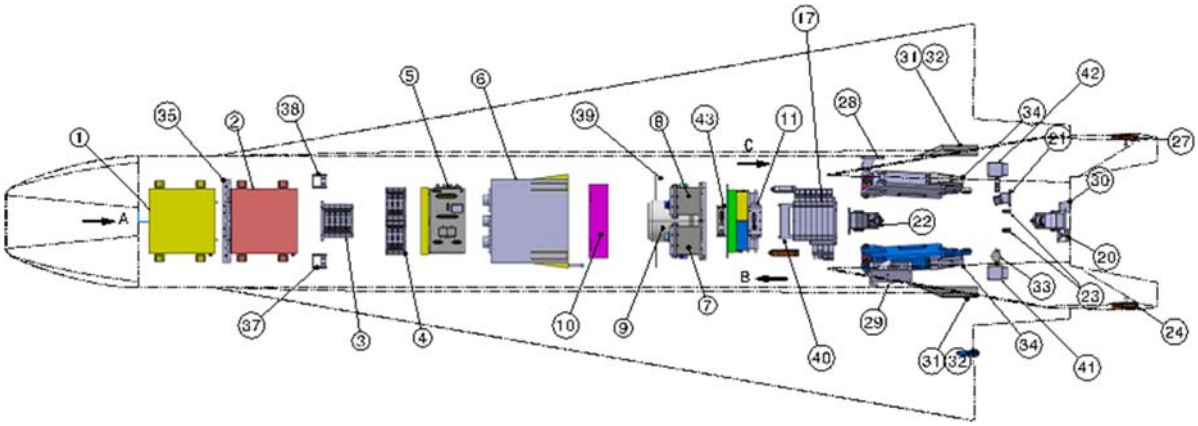

*Fig. 6: Overall EFTV internal Layout*

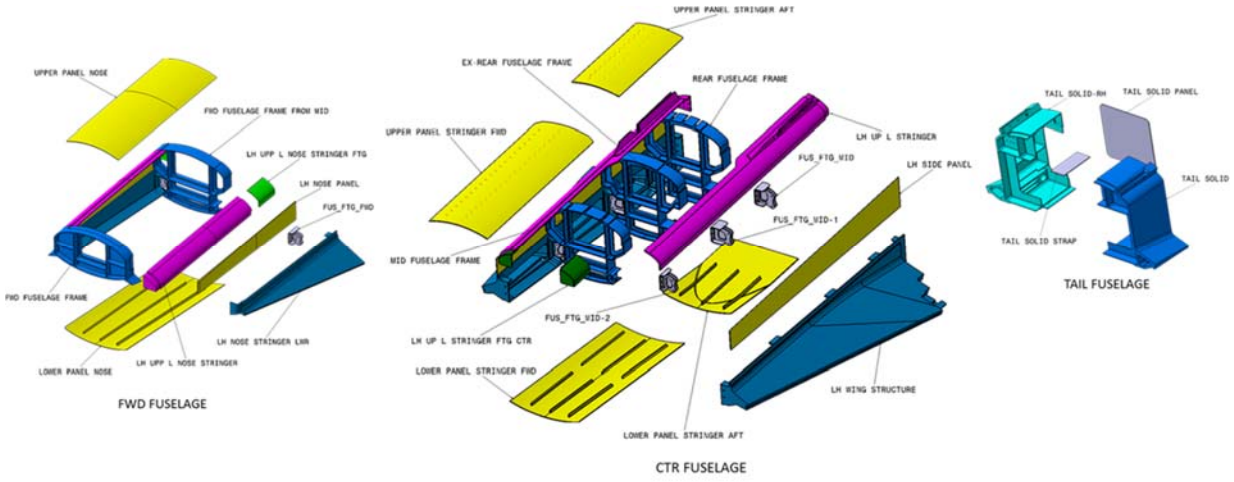


*Fig. 7: Exploded view of EFTV*

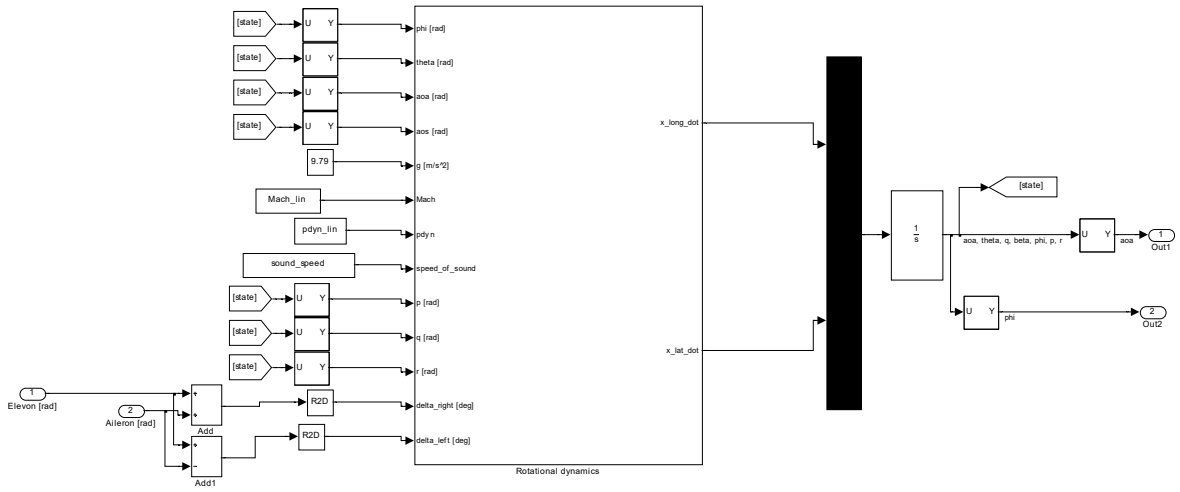


*Fig. 8: Flight dynamics model in Matlab/Simulink*

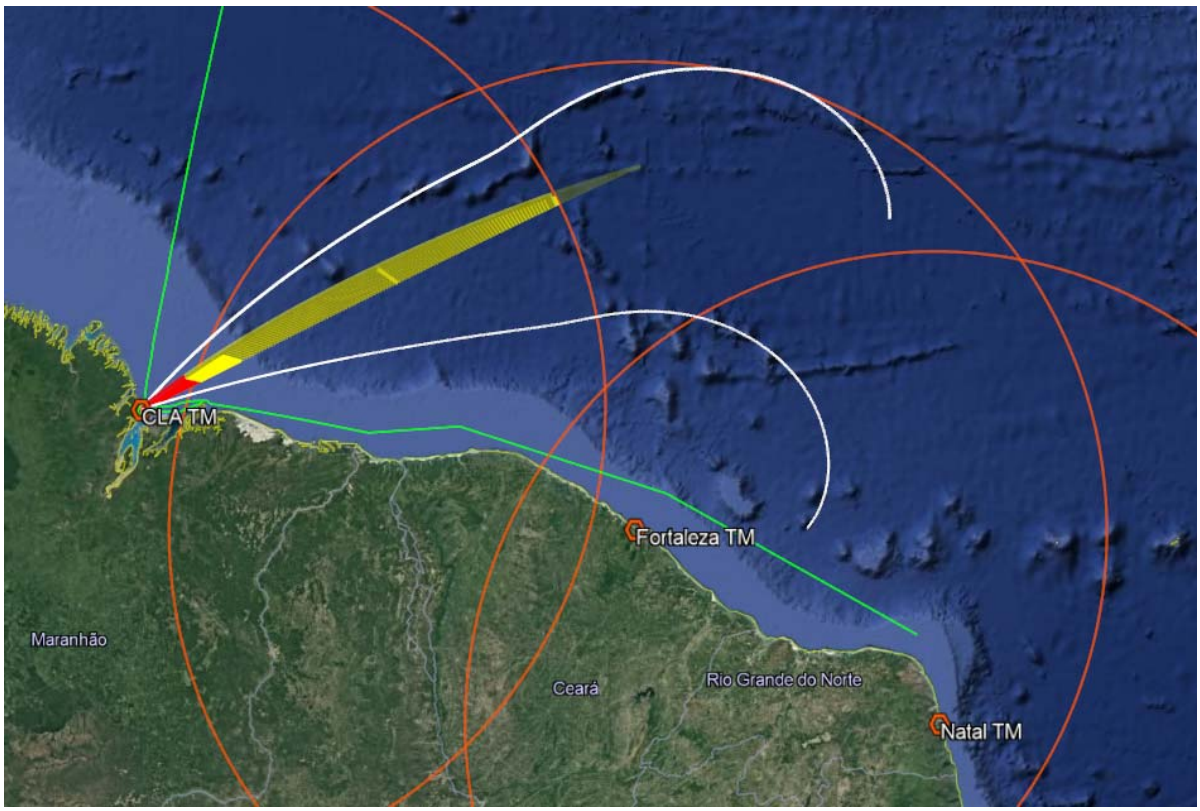


*Fig. 9: Hexafly-INT ballistic trajectory based on VS-50 single-stage at 65° launch azimuth (yellow, S50 burn-phase in red, ballistic flight-phase after ESM separation at 55 km altitude and 600 km down range in grey); 600 km circles indicating coverage of TM stations at CLA, Fortaleza and Natal (orange); preliminary overall trajectory incl. experimental gliding phase based on VBS-43 at 56° and 80° launch azimuth (white)*

One the most critical specifications is the maximum hinge moment that the actuation system should be able to withstand during the pull-out manoeuver. A value of nearly 300 Nm was used for sizing the complete actuation system (see Fig. 10). The elevon and the main portion of the torsion bar are designed as a single CMC block. The CMC bar passes through the fuselage bearing and ends with a titanium insert providing an interface with the titanium lever arm.

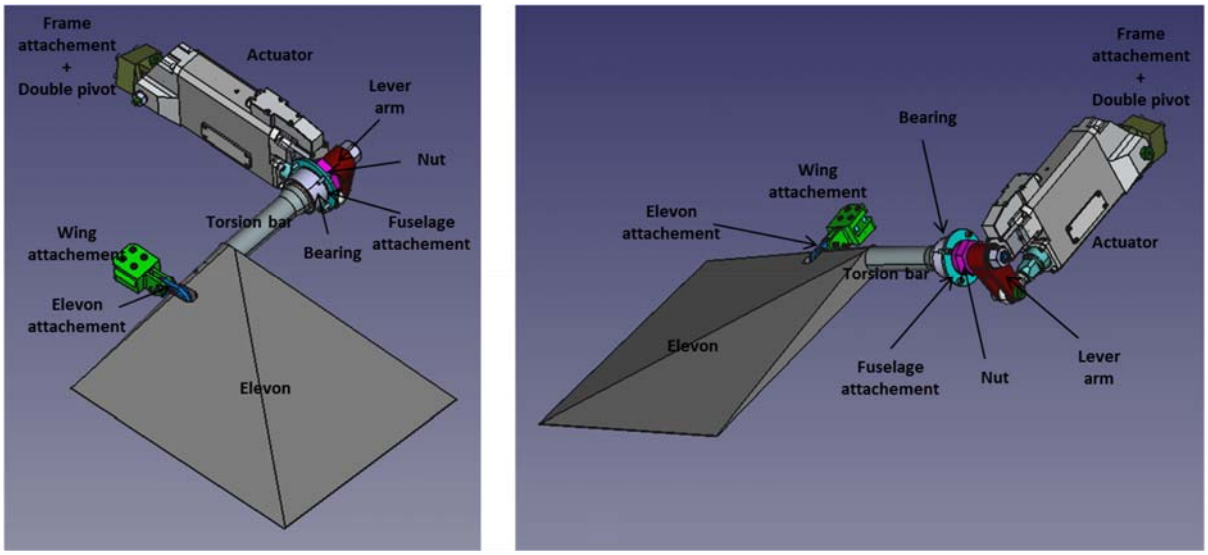


*Fig. 10: Actuation System general design*

Experimental tests indicated that the CMC torsion bar would be able to withstand above 400 Nm before failure. The French ISP society was selected to provide off-the-shelf servo-actuators, customized to withstand all mechanical loads and vacuum conditions. A ground test bench was defined and manufactured so as to check the functionalities of the actuator and ECU in terms of amplitude, speed and acceleration of the motion while some hinge moment (up to the critical value) is applied at the extremity of the torsion bar. This moment is applied thanks to a torque resulting from the deformation of a copper bar aligned with the torsion bar and fixed on the bench at its extremity. The test bench was placed on a vibration table to check the strength with respect to sinusoidal and random vibrations along the three directions. The tests were successful (Fig. 11). The test bench was also used to check in vacuum conditions the mechanical strength of the pressurized ECU and the thermal strength of all components with respect to their own heating by Joule effect. The test includes the first 20 minutes of pre-flight operations when the ECU and actuator are just switched ON and then includes a series of commanded motions which are very conservative in terms of consumed power with respect to the reference flight trajectory. Further details are provided in [23].

*Fig. 11: Test bench for functional tests of the actuator (left) mounted on vibration table (right)*

The qualification of the CMC components and in particular the aileron is planned to be performed in the vitiated C16VK facility at CIAM. CIAM assessed the optimal position of the windtunnel model with respect to the Mach cone generated by the Mach 6.36-6.76 nozzle of the C16VK facility. Different AoA values ranging form AoA = $-5^0$ to $8^0$ were assessed along with three elevon deflections: $-10^0$, $0^0$, $20^0$ (*Fig. 12*). A maximum hinge moment of 315Nm for 49bars total pressure can be realized at AoA=$8^0$ for an elevon deflection of $20^0$ at 49bars of total pressure.

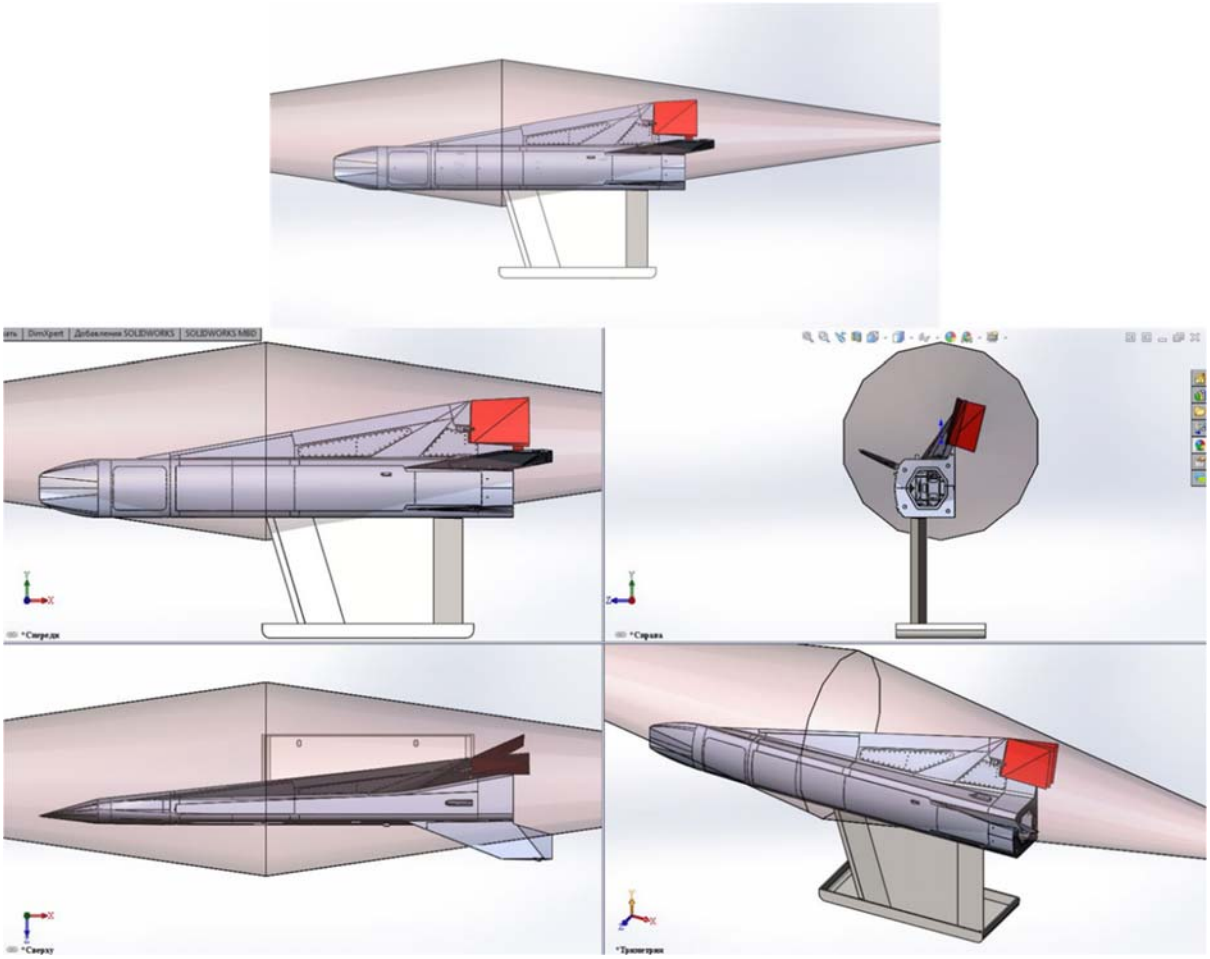

*Fig. 12: Integration of glider windtunnel model at AoA = $0^0$ in C16VK*

To guarantee the lateral stability, two large vertical tails are mounted on the rear. As they are constructed entirely from Titanium, it is necessary to minimize their weight by topology optimization, i.e. finding find the best location to place structure in a pre-defined design domain that is subjected to known loading and boundary conditions. The final structure (Fig. 13) was determined by optimising for all 12 load cases and implementing non-designable regions towards the trailing edge where the thickness of the fin goes below a certain value such that manufacturing cut-outs in this region is not feasible and near the dovetail where cut-outs are not permitted. The final mass of the vertical fin is 12.8kg, this is a 45% weight reduction, resulting in a total weight saving of 20.88kg. The maximum stress found in the proposed vertical fin design is 412MPa occurring at t=47s after the release of the EFTV from the ESM. Further details can be found in [24].

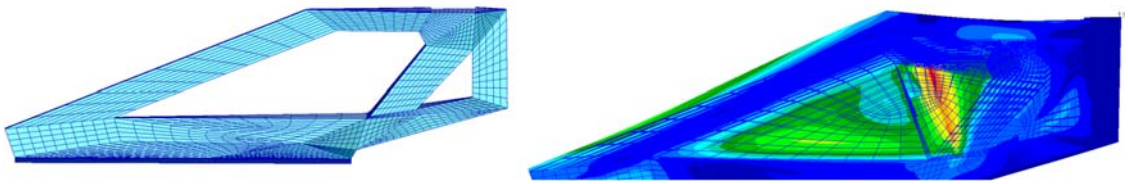

*Fig. 13: Proposed final internal structure for vertical fin (left) and stress distribution at max. stress*

### 1.3.1.3 In Flight Measurement

The EFTV vehicle is equipped with various sensors, which are processed on-board and instantaneously transmitted to the ground. The sensor positions are shown in Fig. 14 and entail heat flux (HF), thermocouples (TC), Pressure ports (PP), Strain gauges (SG), Coaxial Thermocouple (CT) and accelerometers (AC). A particular set is related to the Flush Air Data System (FADS), which consists of 10 pressure ports in the nose.

They will serve as post processing the attitude of the vehicle. The overall cabling is simplified by using breakout boxes, which connect, collect and distribute the data and power from the DAQ boxes to the sensors. For integration of the sensors and data acquisition equipment a mock-up was build and prepared for integration. This mock-up is used to test cable routing, sensors, accessibility, integration concepts and general design of the instrumentation concept for the vehicle in real dimensions without the need of the actual EFTV: Also transfer from the instrumentation from the mock-up to the EFTV will be simplified with this approach. In the *Fig. 15* below, the mock-up for the integration of the IFM equipment is shown.

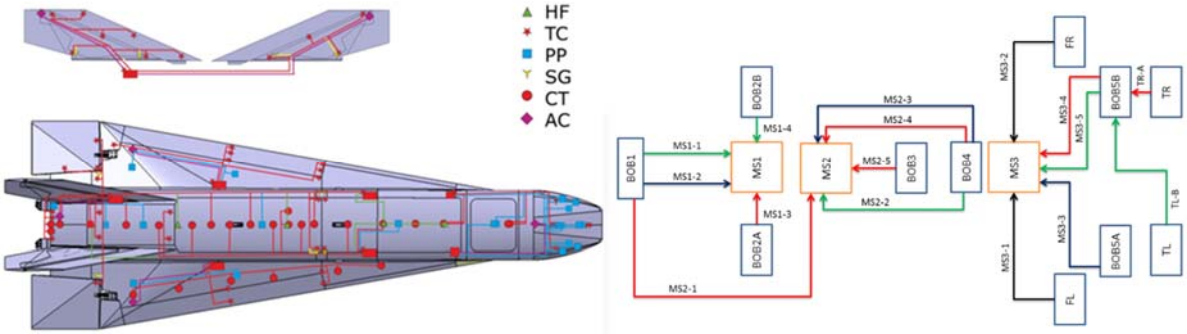


*Fig. 14: Cabling and positioning schema of the sensors (left) and Harnessing within BoB and MS (right)*

*Fig. 15: Mock-up of the EFTV*

### 1.3.1.4 Thermal Management

As a low cost demonstrator, the main structure of Hexafly-Int vehicle is mostly metallic. The chosen material is a Russian variant of titanium alloy, named BT-20, which is able to withstand 700°C and even higher values for shorter periods along the reference trajectory. The assessed solutions for the external Thermal Protection System (TPS) were: (i) heat sink by increasing the titanium thickness (ii) Prosial ® coating (iii) zirconium coating (iv) high emissivity black paint (ε>0.8).

A high emissivity paint (ε>0.8) was found as a sufficient solution for maintaining the temperature of the fuselage panels below 700°C. This paint even allows further reducing the thickness of the leeside panels. At stagnation regions such as the copper nose, root wing and the Ti-leading edges of the vertical tail, additional protection by ZrO2 is needed.

Heating of the internal titanium structure along the trajectory was assessed in [8][9][15]. Fig. 16 shows the maximum temperature distribution obtained for the frames. They were considered not too hot allowing internal equipment to be fixed directly onto them.

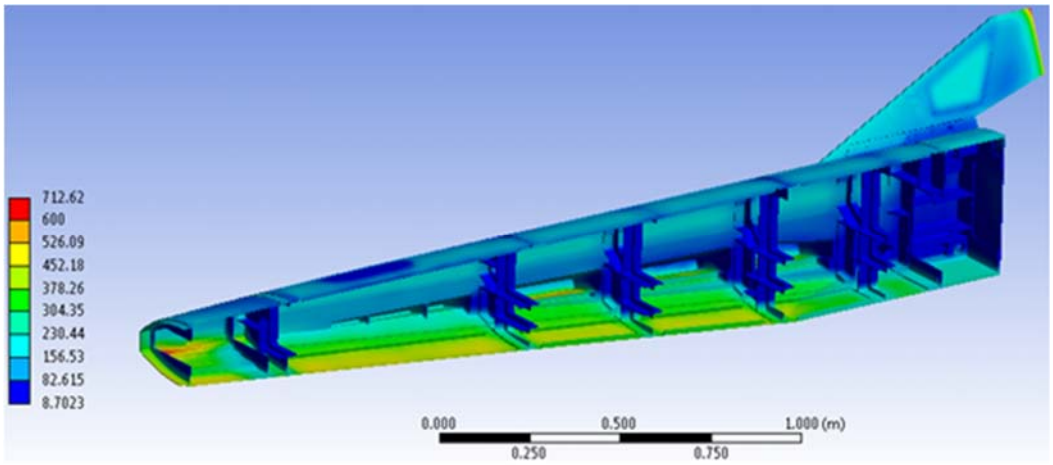


*Fig. 16: Maximal temperature distribution on the titanium internal structure*

The main source of equipment heating is the thermal radiation coming from the panels of the structure. ONERA and ESA designed an internal thermal protection system based on a light flexible microporous insulator named Aeroguard® provided by PROMAT firm in Belgium. This material is able to withstand 1000°C and it exhibits an extra low thermal conductivity at sea level and is even further reduced at high altitude (lower pressure). The thermal control system is composed of different layers of Aeroguard 190 ® panels, which are attached with lateral Velcro traps fixed at their extremities to the internal frames of the structure (*Fig. 17*). This smart fixation allows fast depressurization of the insulation panels and optimization of the mass while withstanding mechanical vibrations during the boosted phase of the flight. Tests have been performed by VKI in the ESA-ESTEC Large Diameter Centrifuge (see *Fig. 17*) up to 16g. Aeroguard® panel was tested under acceleration in any direction. The detailed discussion on thermal management is worked out in [22].


*Fig. 17: Customized internal thermal protection system fixation with Velcro (left) and testing under acceleration (right)*

### 1.3.1.5 Aerodynamic Performance

#### 1.3.1.5.1 Numerical Aerodynamic Evaluation

The numerical aerodynamic database generation is carried out by CIRA, DLR, ESA and TsAGI. In the early design phase, only inviscid CFD computations were performed and a preliminary AErodynamic DataBase (AEDB) of the EFTV configuration was setup by DLR-Braunschweig [11] with the goal to provide aerodynamic performance for the first Flight Mechanics analyses and to check the vehicle longitudinal and lateral-directional static stability. In fact, it had to be verified that vehicle aerodynamic surfaces were able to provide sufficient lift at hypersonic atmospheric entry to stay within the load constraints during descent and reach the envisaged altitude corridor to realize the first phase objectives. Aerodynamic coefficients were provided as a function of Mach number, angle of attack, sideslip angle, and aileron deflections.

The Mach range from 2 to 9 was analysed for the EFTV only in the continuum regime with air modelled as an ideal gas. An example of inviscid aerodynamic assessment is shown in Fig. 18. As summarized in Ref. [11], the EFTV aeroshape features rather high lift-to-drag ratios at hypersonic speeds. No significant effects of sideslip on aerodynamic efficiency and total pitching moment for both clean and deflected aileron configurations were predicted. Numerical results clearly underline that the glider is statically stable in longitudinal flight at all Mach numbers under investigation and for all the angles of attack, sideslip, and aileron deflections considered so far.

Further, results also pointed out that the aeroshape seemed to be trimmable in all the flight conditions investigated [11], also for supersonic Mach numbers and higher angles of attack. Finally, static stability in lateral-directional flight conditions is also confirmed since at all Mach numbers it is verified that $C_{Y\beta}<0$, $C_{n\beta}>0$ and $C_{l\beta}<0$ (the last one only for positive angles of attack) [11]. As a conclusive result, the preliminary AEDB pointed out the compliance of the hypersonic glider's aerodynamic performance with the expected flight envelope.

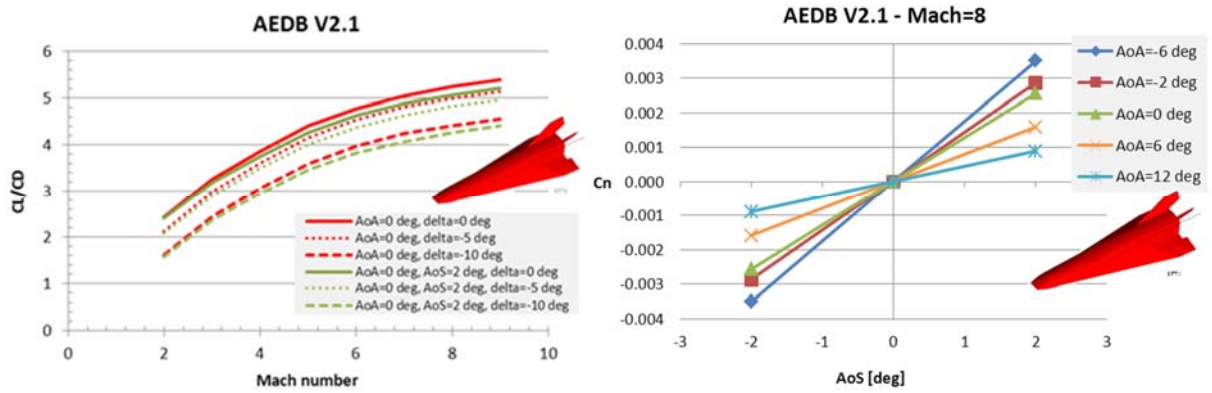


*Fig. 18: The L/D vs. Mach (left) and yaw moment coefficient versus sideslip (right) at different attitudes.*

The preliminary mission trajectory was generated by DLR-Moraba for the ascent phase assuming a total payload mass of 800kg (EFTV, ESM, launch vehicle service module, fairing). The descent trajectory was assessed by GDL considering a "train" EFTV+ESM from apogee down to 55km altitude and then followed by only the EFTV after its separation from the ESM. A number of 3 degree-of-freedom (DoF) planar trajectories were generated for the hypersonic glider. EFTV's AoA initial schedule was based on a profile that satisfies control authority criteria. Trajectory labelled B-viscous (see Fig. 19) was finally selected as reference, being the lower reference trajectory of the flight corridor having a built-in margin during future trajectory consolidation, and preliminary EFTV/ESM separation was fixed at 55km altitude to satisfy typical control authority criteria.

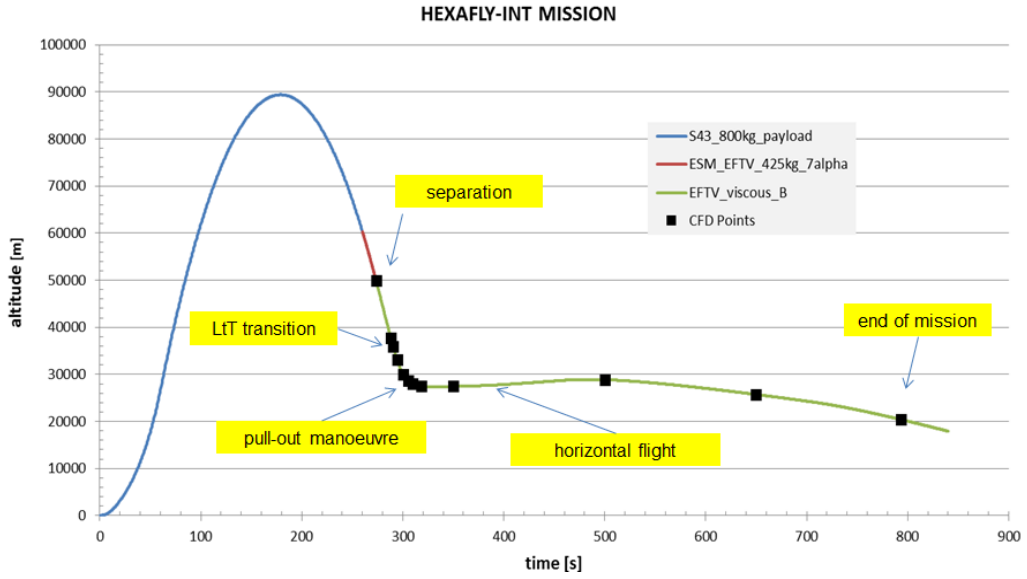


*Fig. 19: Reference trajectory: altitude time history.*

CIRA, ESA and TsAGI have finalized Navier-Stokes (NS) CFD simulations to generate the final viscous AEDB. More than 250 3-D Navier-Stokes simulations were carried out in laminar and fully turbulent flow conditions (Spalart-Allmaras one-equation eddy viscosity is being selected for turbulence modelling). Those CFD simulations are conceived to address the effects of Mach number, angle of attack, angle of sideslip, symmetric and asymmetric aileron deflection, Reynolds number, grid resolution, turbulence models, laminar-to-turbulent transition, code-to-code, and finally to verify trim conditions and aero-thermal loads along the reference trajectory. The AEDB includes also the model of uncertainties for aerodynamics and the dynamic derivatives data-package, thus providing inputs for flight mechanics, thermo-structural analysis (the aero-thermal loading conditions the EFTV has to withstand during the flight must be accurately verified) and in-flight experimentation layout optimization.

An exemplary hybrid computational grid (i.e. tetrahedrons in the flow and prisms inside the boundary layer) built for NS simulations is shown in Fig. 20. At least 10 million cells were necessary for a half configuration, and in the case of turbulent boundary layer assumption, the condition of $Y^+$=O(1) at wall was imposed. Surface temperature contours on the full vehicle during the descent and the effect of sideslip at high angle of attack, at Mach=7.5 are shown in Fig. 20. The hot nosetip, wing leading edges and fin leading edges as result of nearly attached shock waves are noticeable. From laminar boundary layer parameters extracted from CFD results to apply local natural and step-induced transition criteria along the reference trajectory [13], a fully turbulent flow was proposed at the altitude of about 30 km. More details on the aerodynamic database and related uncertainties can be found in [12][26].

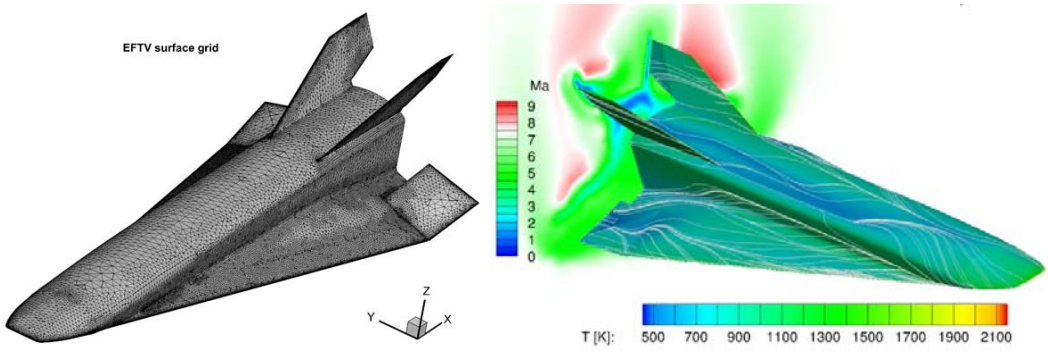


*Fig. 20: Hybrid NS mesh (left) and EFTV surface temperature contours and skin-friction lines (Mach=7.5, AoA=10°, AoS=4°, clean configuration).*

### 1.3.1.5.2 Experimental Aerodynamic Evaluation

The experimental test campaign on the aerodynamics of the EFTV glider configuration was performed at TsAGI in the supersonic and hypersonic wind tunnel T-116, characterized by a test chamber with a squared cross section of 1 m × 1 m size. The tests were performed with the model produced by TsAGI, whose scale was 0.35 w.r.t. the size of the EFTV. The model (Fig. 21) has allowed investigating aerodynamic characteristics of the vehicle with different settings of aileron's deflection.

*Fig. 21. The model of the EFTV Glider Option mounted on a sting.*

The windtunnel campaigns in the T-116 at TsAGI have been performed in a Mach number range from 3 to 8 at angles of attack from – 6º to 12º. The freestream conditions are reported in Table 2 in terms of Mach number, total pressure $P_{tot}$, total temperature $T_{tot}$ and unit Reynolds number $Re_{1m}$. The latter is adapted to the flight altitude $H$ of the real EFTV vehicle and the model scale. The test conditions in T-116 are reasonably close to those expected along the flight trajectory of the EFTV vehicle (Fig. 19).
An electromechanical balance measured the aerodynamic forces and moments. To correct for the sting in the rear, the base drag was excluded from the experimental data by measuring the base pressure on the model. Corresponding corrections were made by equalizing the base pressure to the free-stream static pressure. Corrections were also made for taking into account the effects of gravity and sting deformation during tests.

Table 2: Flow conditions used in the Wind Tunnel T-116

| **Mach** | **3.03** | **4.05** | **5.05** | **6.00** | **6.99** | **7.88** |
|---|---|---|---|---|---|---|
| **$P_{tot}$ [atm]** | 1.1 | 1.4 | 5 | 7.4 | 22 | 31.5 |
| **$T_{tot}$ [K]** | 300 | 300 | 455 | 485 | 675 | 825 |
| **$Re_{1M}*10^{-6}$** | 7.74 | 5.96 | 6.88 | 6.32 | 7.66 | 5.92 |
| ***Simulated Flight Altitudes:*** | | | | | | |
| **H [km]** | 24.8 | 28 | 28.4 | 30.5 | 30 | 32.5 |

The main aerodynamic characteristics of the glider model without flap deflection and zero sideslip angle, i.e. aerodynamic drag force coefficient $C_D$,, aerodynamic efficiency $L/D$ and pitching moment coefficient $C_m$ are presented in Fig. 22 as function of angle-of-attack $\alpha$. The reference parameters used for calculating the aerodynamic coefficients were the model plan-form area $S_{ref}$=0.3087m$^2$ and the model fuselage length from the leading edge of the nose cap to the base section $L_{ref}$=1.15m. The moment reference centre MRC of the model corresponded to 57% of the fuselage length. The maximum values of aerodynamic efficiency change from 4.5 to 4.0 with increasing Mach number from 3 to 8 whereas the stability in pitch decreases. The pitching moment coefficient $C_m$ at Mach numbers 4 and 7 and different angles-of-attack are shown in Fig. 23 for a range of symmetrical aileron deflection angles $\delta$ = –18°…+6°. For the considered MRC position, the EFTV can be trimmed in pitch for angles-of-attack ranging from –6° to +6° by symmetrical flap deflection from +2.5° to –16° at Mach number $M$ = 4, and from +4° to –12° at $M$ = 7.

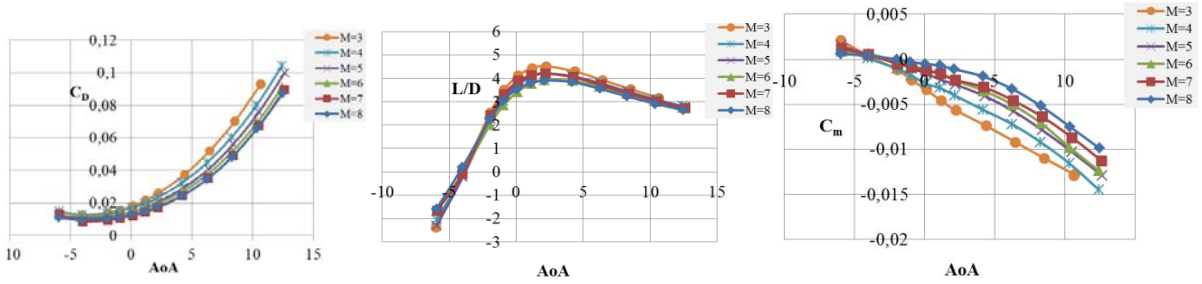


*Fig. 22: Drag force coefficient $C_D$, aerodynamic efficiency L/D and pitching moment coefficient $C_m$ of the glider vs. angle-of attack α. δ = 0º.*

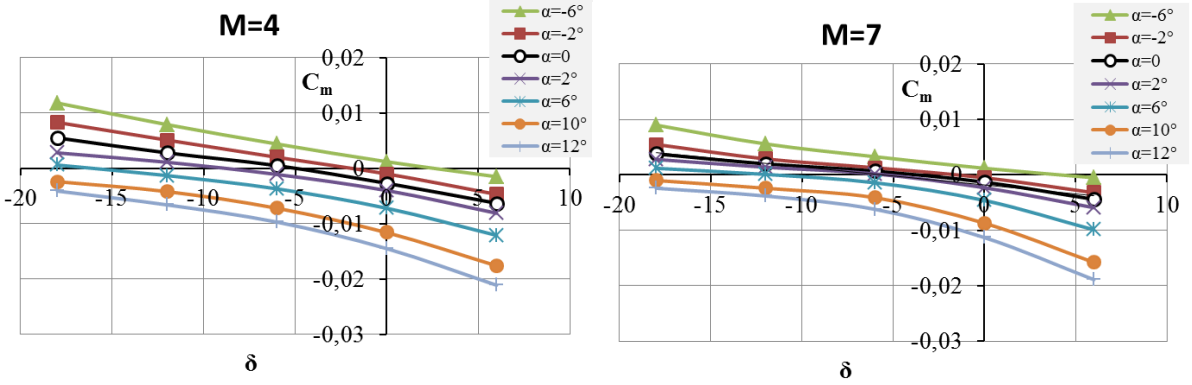


*Fig. 23: Pitching moment coefficient of the glider model $C_m$ vs. symmetrical flap deflection angle $\delta$.*

Additional experimental tests in T-116 were devoted to hypersonic boundary layer transition (BLT) with and without different transition grits installed near the nose/fuselage junction. A detailed description of the methodology and the results are presented in [13]. These tests were provided primarily at Mach number M=7. As an example, the photo of the forward part of the model with the transition grit consisting of cylindrical screws of 2mm diameter and the results of tests with different heights of screws k=0.35, 0.7 and 1.4mm are presented in Fig. 24. The points represent the experimental Stanton numbers obtained during tests in the symmetry plane on the windward side vs. local Reynolds numbers, whereas the lines correspond to calculated theoretical station values for laminar and turbulent boundary layers. Without any transition grit, the boundary layer is laminar for more than half of the model length, while transition grits promote BLT significantly earlier. The results were used to predict the position of BLT zone and heat transfer levels during the flight test.

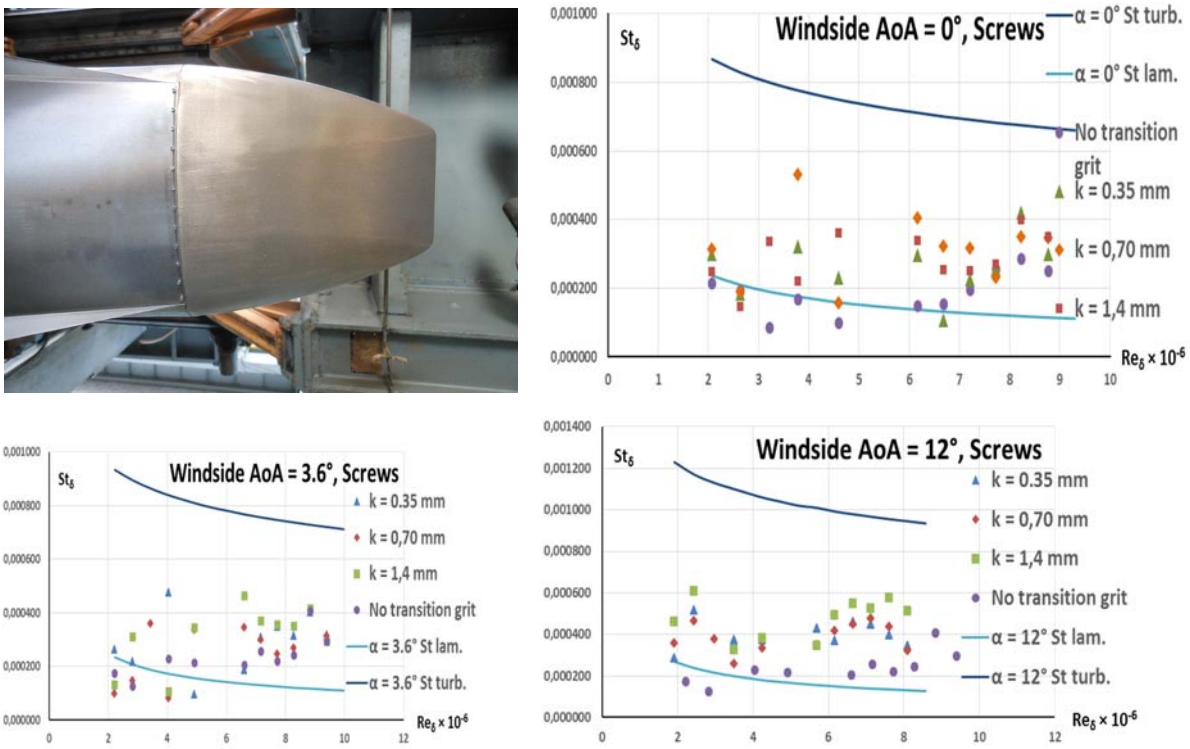


*Fig. 24: Model with transition grit installed (top left) and Stanton numbers vs. local Reynolds number; M = 7.*

In parallel, the potential occurrence of transition triggered by irregularities or imperfections at the sharp leading edges was investigated in the HEG shock tunnel of DLR at Göttingen by means of temperature sensitive paint (TSP). Rather than protuberances creating perturbations in the boundary layer, a large induced inviscid vortex was triggered at the root of the leading edge resulting into an increase heat transfer on the windward side (Fig. 25). This was confirmed by detailed CFD analysis where Fig. 26 provides the estimated relative surface heat flux increase on EFTV assuming a fully laminar boundary layer and an unimpaired vortex.

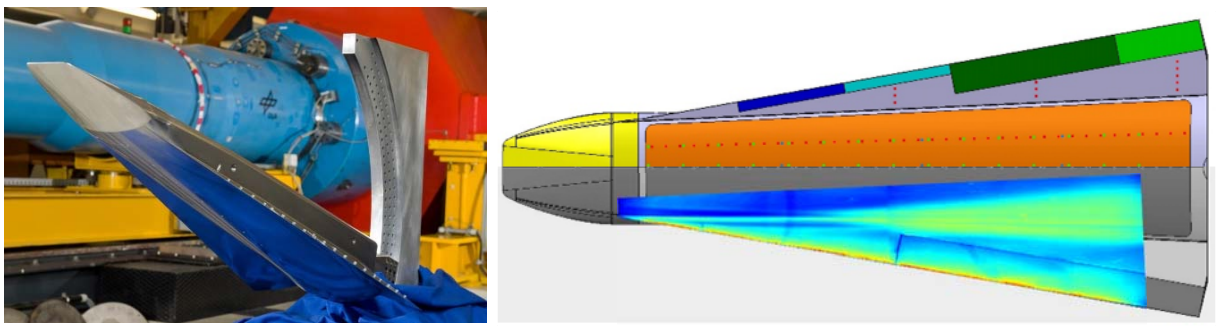

*Fig. 25: Windtunnel model in front of HEG (top left) and the related wedged heat transfer increase.*

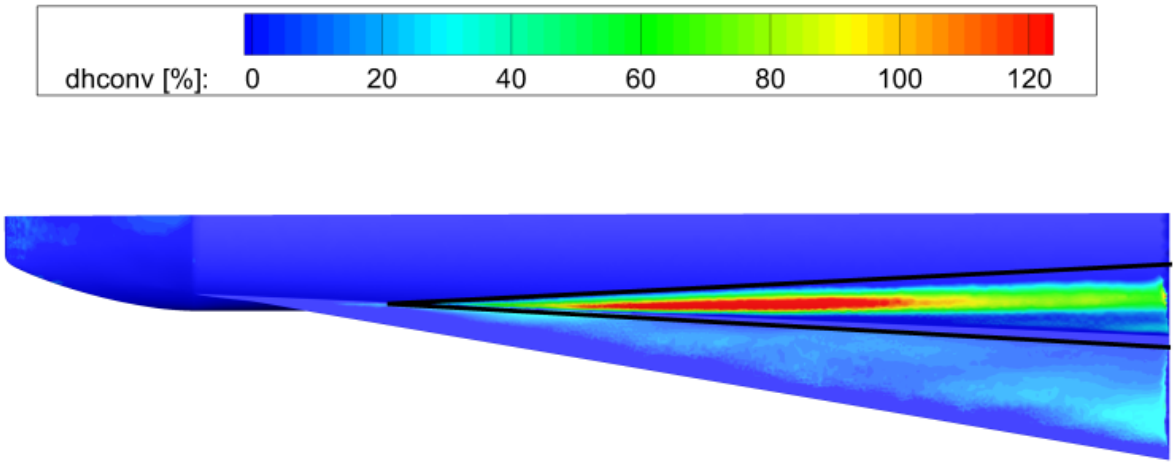


*Fig. 26: Relative surface heat flux increase due to the presence of the vortex (no break down) at AoA=12deg. (ESA CFD, total model length 2.5 m)*

The effects of gaps between the CMC leading edge segments can also induce transition. The maximum gap sized between the leading edge segments was estimated based on a thermo-structural evaluation by DLR Stuttgart. The maximum gap sizes together with the relative direction of motion are indicated in *Fig. 27*. The imposed gaps did not cause a heat flux increase at the transducer locations on the wing.

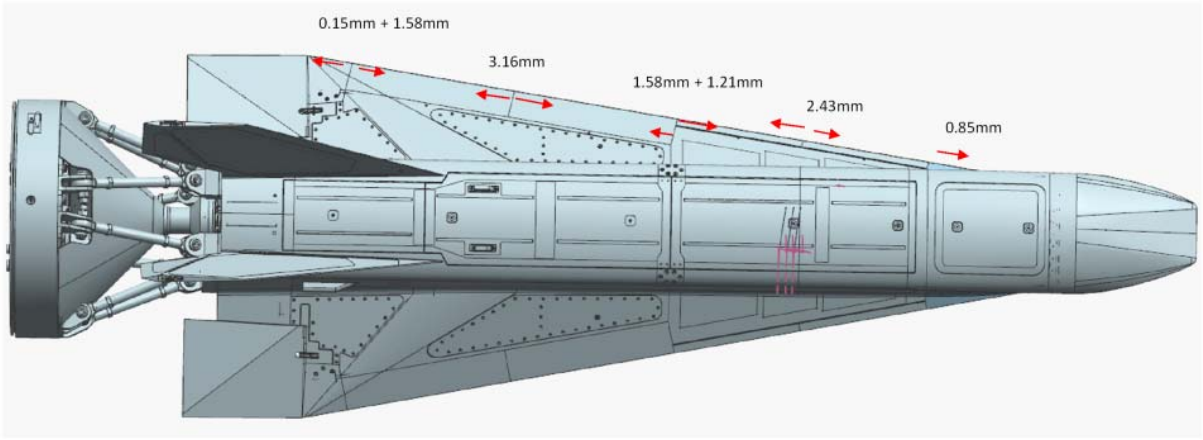


*Fig. 27: Estimated maxima gap sized based on a thermo-structural analysis.*

### 1.3.1.6 EFTV/ESM Stability and Separation

An aerodynamic database for the HEXAFLY train (EFTV + ESM) has been constructed for two flap deflection angles of the EFTV. The increase of the flap deflection from 0° to 10° is needed to keep the vehicle trimmed in the case of shifting the MRC of the train rearwards. *Fig. 28* shows on the left hand side the $C_m$ data versus AoA for the original MRC and on the right hand side the data for a rearward shifted MRC. For a flap deflection angle of 0° the trimmability margin is very low.

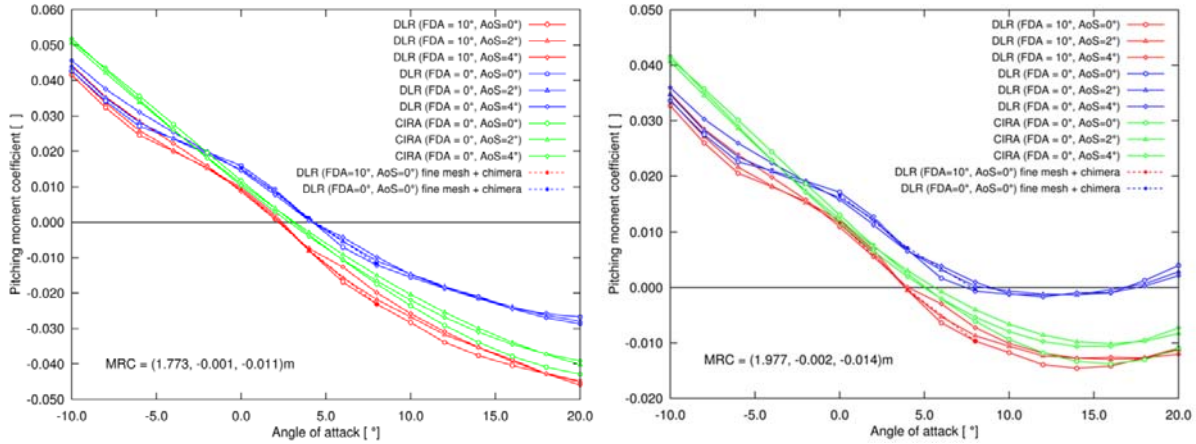


*Fig. 28: Comparison of the pitching moment coefficient Cm versus angle of attack AoA with existing data from CIRA (green lines) and DLR separation results (dashed lines) for the original MRC (left) and a rearward shifted MRC (right).*

To assure a clean separation between EFTV and ESM, the separation event was simulated for a flight Mach number of 6.9 at an altitude of 55km once the EFTV has the full aerodynamic control authority. The motion of both vehicle segments (EFTV and ESM) was simulated in an initial geodesic coordinate system. In former simulations only the motion of the ESM relative to the EFTV was taken into account. Starting from a steady-state initial solution with free-stream and flight state, an unsteady CFD/RBD simulation was initiated where both vehicles execute a 6DoF motion. The time step for the inviscid simulation is 5 ms and five coupling cycles were performed; the computational grid for the EFTV and ESM contains 61.4 and 20.5 million tetrahedrons, respectively. Different cases with an angle of sideslip AoS = 0° and 4° were investigated for the EFTV configuration with a flap deflection angle of FDA = 0° and/or −20°. To make sure that the angular rotation does not lead into a collision, the relative position of both parts were analysed. Fig. 29 shows the relative position and attitude of the ESM to the EFTV in steps of 0.25s after the initiation of the detachment for one of the studied cases. The different initial conditions lead to different pitch and yaw angles, nevertheless no contact either with the protruding vertical fins nor the flaps was detected. A roll motion of the EFTV is observed in the case of 4° sideslip. With -20° flap deflection a pitch-up of the EFTV is observed.

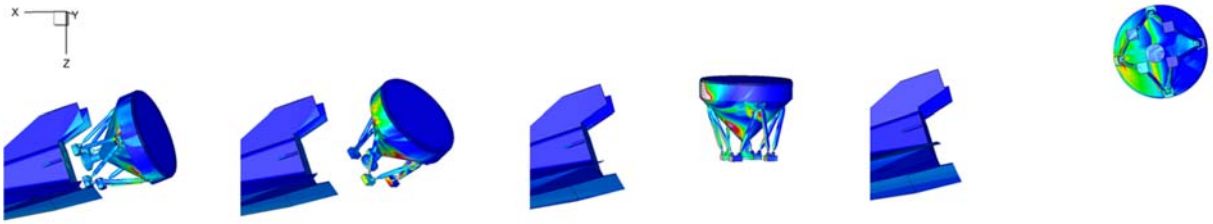


*Fig. 29: EFTV/ESM separation for 0° flap deflection angle and 4° angle of sideslip in intervals of 0.25 s.*

To verify and validate the above simulations, the separation process was also performed experimentally. Dynamically scaled models of the EFTV and ESM are manufactured at sub-scale, instrumented by UNSW with a miniaturized on-board inertial measurement unit (IMU), and flown in the short duration flow of a hypersonic wind tunnel TUSQ while being filmed by a high-speed schlieren optical visualization tool. The miniaturized IMU incorporates a tri-axial accelerometer and a tri-axial gyroscope as well as a dedicated microcontroller, power supply and blue-tooth module for communication. Internal ballast is used to tune the mass, CoG and moments of inertia of the model to ensure that the models are dynamically scaled [17] (see Fig. 30). A number of experimental campaigns were performed in the University of Southern Queensland's hypersonic wind tunnel (TUSQ) [18][19]. This compression-heated Ludwieg tunnel provides approximately 200ms of steady flow, with a start-up period of around 5ms. The model is released to fall under gravity toward the centreline of the Mach 6 nozzle, and then the tunnel is fired to produce the test flow in which the model then flies. The schlieren system provides both high-speed video for image tracking and simultaneous visualization of the flow structure around the model during the flight (see Fig. 30). Results from the image analysis of the free flight experiment and subscale CFD/RBD simulations are presented in Fig. 31 (left). Displacements in the X direction agree within the duration of the separation, as the ESM was detached at approximately 10 ms. As the displacement is calculated frame to frame, any slight measurement error will

accumulate as the model is tracked for longer time durations. The right plot of Fig. 31 shows that the rotation occurs almost immediately. Rotation data from both image analysis and integrated gyroscope measurements show good agreement.

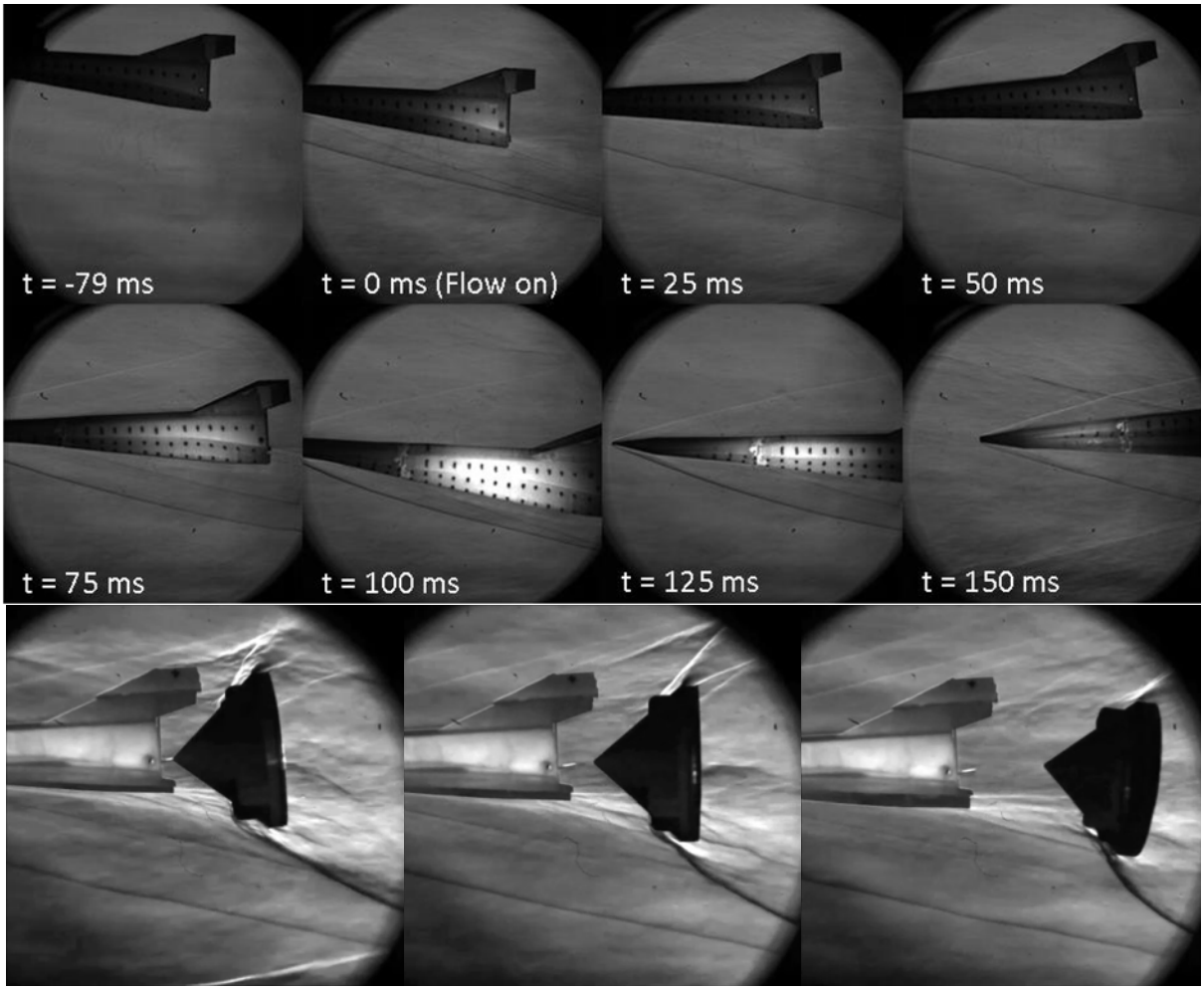


*Fig. 30: Free flight of EFTV (top) and separation sequence of ESM from EFTV (bottom).*

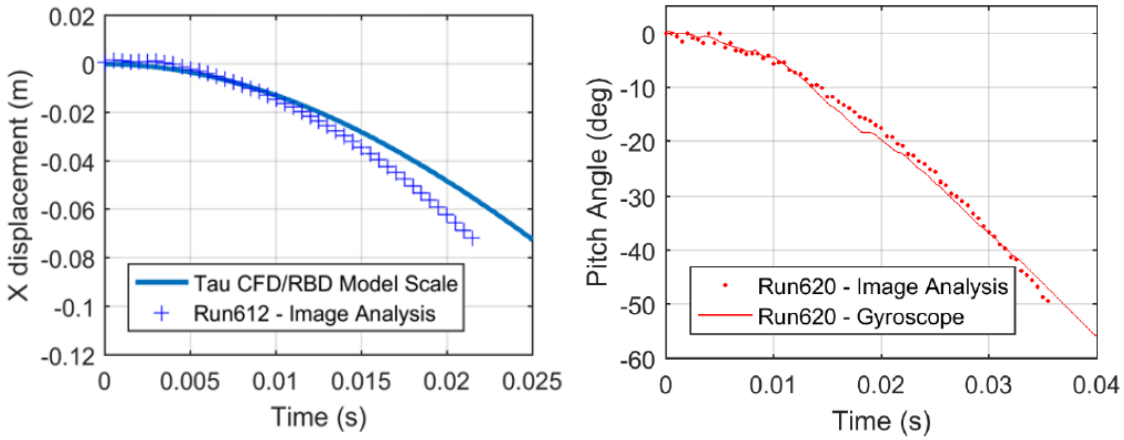


*Fig. 31: ESM dynamics compared to results from CFD/RBD simulation (left) and ESM pitch movement comparison between on-board IMU and image analysis.*

### 1.3.1.7 Sonic Boom

The sonic boom produced by the EFTV is expected to be an N wave with a ground reflected strength of the order 10Pa when the vehicle flies at 2° angle of attack. The result is very similar to the prediction made in HEXAFLY, but the current work was based on the updated geometry and used an in-house CFD simulation with a computational domain tailored for accurate downwash calculation.

The method used to predict the sonic boom signature was originally developed within ATLLAS. An essential aspect of this method is that the signature can be predicted directly from the downwash in the near field. This was previously shown to be true for axi-symmetric bodies, using MOC to derive the downwash flow-field. However, the CFD simulations of flow under winged vehicles provided by partners in previous projects were simply too dissipative, and the predicted shock over pressure at the ground was dependent on where the integral was made. Without proof or at least a demonstration that the integral was invariant for 3D vehicles there remained the possibility that the technique proposed was somehow restricted in application to axisymmetric bodies. The CFD domain is presented in **Error! Reference source not found.**, which extends to about 7 vehicle lengths downstream and 1 below. 2nd-order Euler simulations were performed until both the wall force and solution residuals remained constant. Vertical velocity contours in horizontal planes at z/L=0.304, 0.608 and 0.911 are presented in *Fig. 32*-right (reference length L=3.29, flight Mach number 7.4, angle of attack 2°). Downwash is integrated across the span to calculate the total source function along with the integral of the Whitham function. The maximum of the integral is 0.092±0.0005$m^{3/2}$ at all three planes. It was therefore demonstrated for the first time that the method of deriving the Whitham F function from near field CFD really is applicable to 3D geometry and independent of the distance below the vehicle at which the integration plane is set.

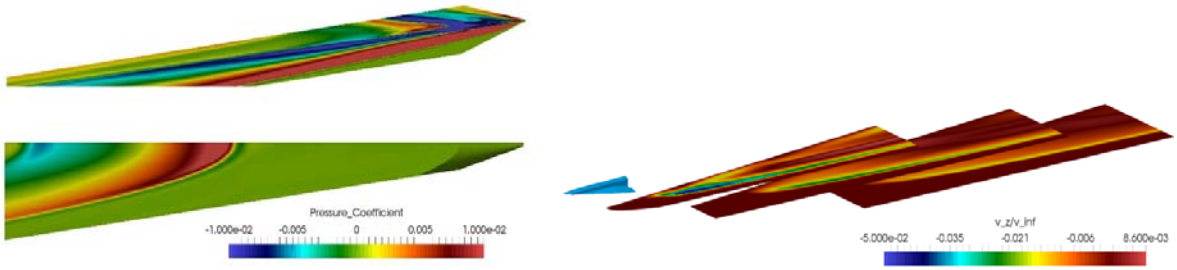


*Fig. 32: Left: Pressure coefficient contours; side view (top) and bottom view (bottom). Right: Vertical downwash contours beneath the EFTV*

## 1.3.2 Low-Speed Flight Concept

### 1.3.2.1 Low-Speed Flight Experiments

As the project foreshadows a high-speed passenger vehicle [16], the EFTV needs to be stable throughout the entire flight envelope. Even though subsonic stability is often overlooked in hypersonic vehicles, it is crucial to obtain a viable final design. The low speed variant to be used for flight-testing was scaled to a length of 1.15m. Thus, the vehicle is large enough to be visible for the ground-based pilot. At the same time, it is small enough to be installed in the wind tunnel. As a propulsive system, an electric ducted fan with a diameter of 90mm is used. In combination with a battery consisting of ten Lithium Polymer cells connected serially, up to 42N uninstalled thrust is provided.

A full-scale wind tunnel model of the flying testbed was fabricated using an assembly of 3D printed pieces, which were then glued together and sanded for a smooth finish. Components such as the elevons and rudders are removable to allow the testing of various control settings. The rear portion of the ducting system was also removable to allow various pressure instrumentation to be installed. The vehicle was mounted using an external adapter to the wind tunnel load cell. Fig. 33 shows the model mounted in the wind tunnel.

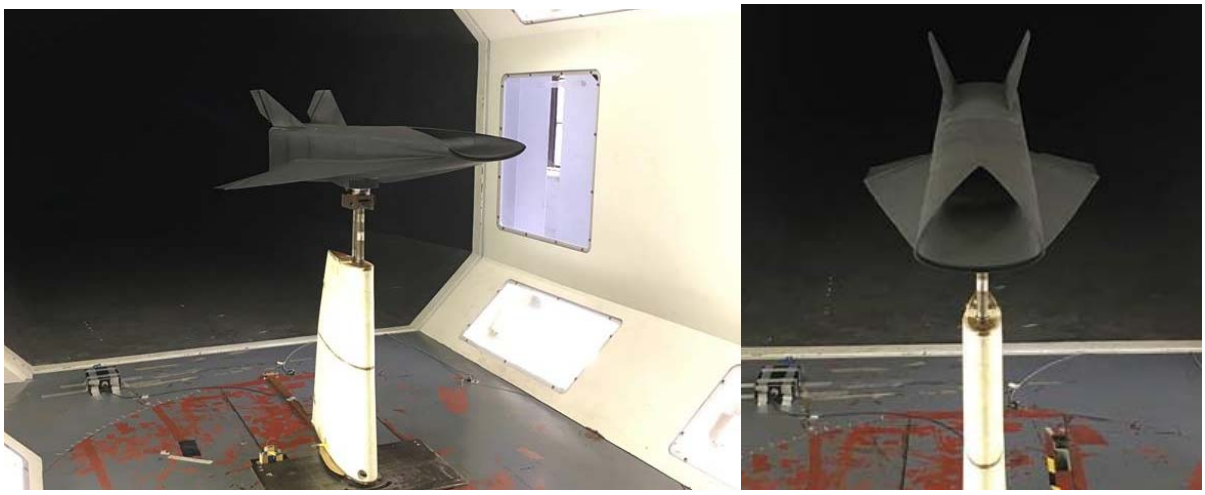

*Fig. 33: Views of Vehicle in Wind Tunnel*

The data acquired during testing was from load cell data to find aerodynamic and static stability coefficients, pressure data to characterise the internal flow path and tuft flow visualisation to determine the lip flow separation tendencies. Tests were conducted both with and without the fan installed to analyse its effects. During selected runs, total and static pressure measurements were taken to determine the nozzle jet velocity, flow quality at the fan face as well as the static pressure jump across the fan.

Fig. 34 shows the drag force variance with increasing airspeed based on the aircraft properties presented in Fig. 34. Cruise speed is selected to keep AoA below $5^0$ while being speed stable. For this reason, a cruise speed of 21m/s is selected. The aircraft can be trimmed in this condition with $-5^0$ of elevon deflection. A take-off speed is determined to be ~16.5m/s at an AoA of $8^0$. For landing, the AoA could be increased to lower the speed further than at take-off. Finally, the Oswald Efficiency Factor is 0.796, which is within the range of other delta-winged aircraft.

Fan tests were run to determine the installed thrust. *Fig. 35* shows significant losses in thrust when increasing the AoA or the airspeed. The maximum thrust loss is ~46% for the lower power setting, as the fan begins to windmill and the flow separates from the intake lip. The higher power setting results in only ~ 27% thrust loss as the fan windmills less and extra suction delays the lip separation. Looking at Fig. 34 above, the thrust setting for a 10S Lipo system would be approximately 15A (between the two power settings shown below).

Both CFD and wind tunnel tests have confirmed the presence of a vortex originating at the top lip of the intake, which is ingested by the fan. This vortex is present at all tested airspeeds and AoA, but its location varies. Fig. 36 shows the CFD model for the vehicle at $0^0$ AoA and a fan setting of 20A running on 8S lipo. The wind tunnel results compare well with CFD, showing the presence of these dual vortices. This may affect the fan performance when compared with an ideal inlet. The overall layout and implementation trade-offs are described at length in [25].

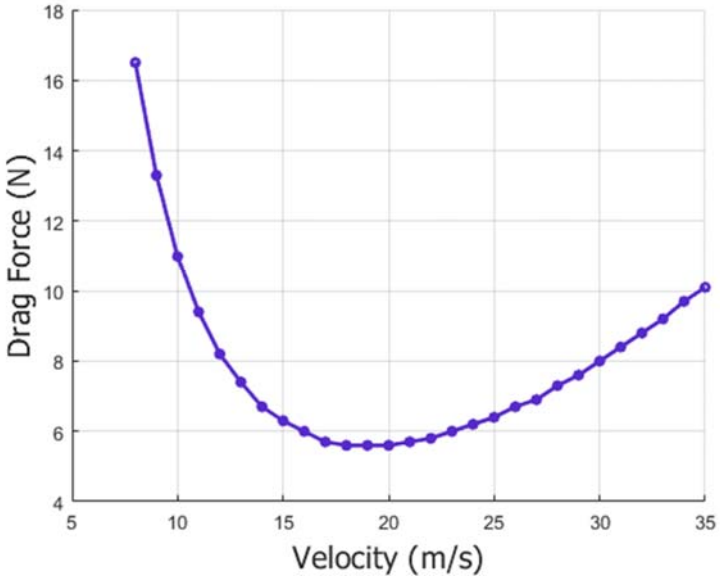


*Fig. 34: Drag vs. velocity results for airframe only.*

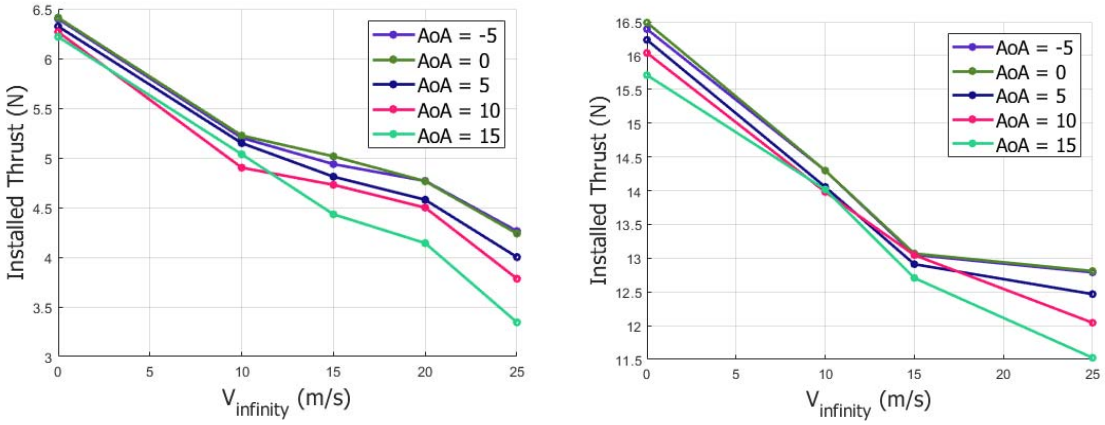


*Fig. 35: Installed Thrust for 10SLipo with 10A (Left) and 20A (right)*

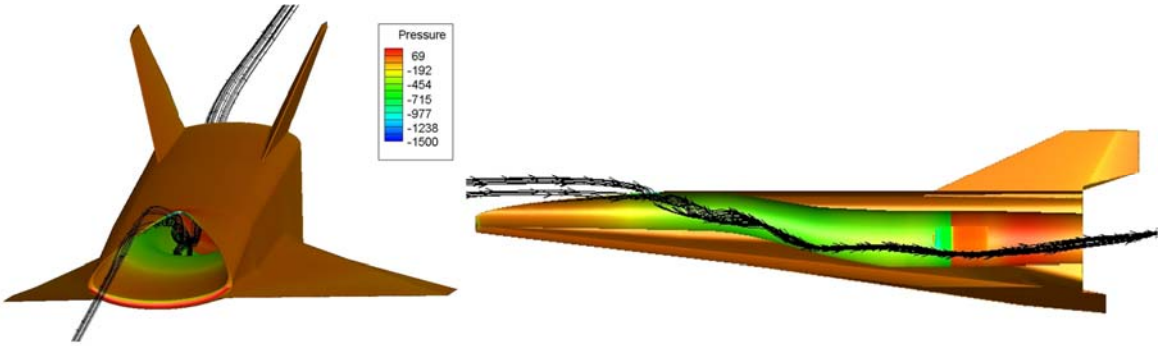


*Fig. 36: Vortex originating from top inlet lip is ingested by the fan at $0^0$ AoA and a fan setting of 20A*

### 1.3.3 High-Speed Powered Concept

#### 1.3.3.1 Aero-Propulsive Performance of the Powered Vehicle

TsAGI performed CFD studies of the 3m-long EFTV scramjet propelled configuration developed earlier within the European HEXAFLY Project [7]. Both laminar, transitional and turbulent simulations were performed. Numerical simulations have been conducted in the range of $M_\infty$ =5÷8 and AoA = -2°÷8°. The Reynolds numbers calculated on the airframe body length correspond to the following values: $Re_L=6.88\cdot10^6$ ($M_\infty=5$), $Re_L=5.38\cdot10^6$ ($M_\infty=6$), $Re_L=7.66\cdot10^6$, $Re_L=7.33\cdot10^6$ ($M_\infty=7$) and $Re_L=5.92\cdot10^6$ ($M_\infty=8$). The computational grids of approximately 15 million elements are shown Fig. 37 where the intake area and the beginning of the internal propulsive path are also detailed.

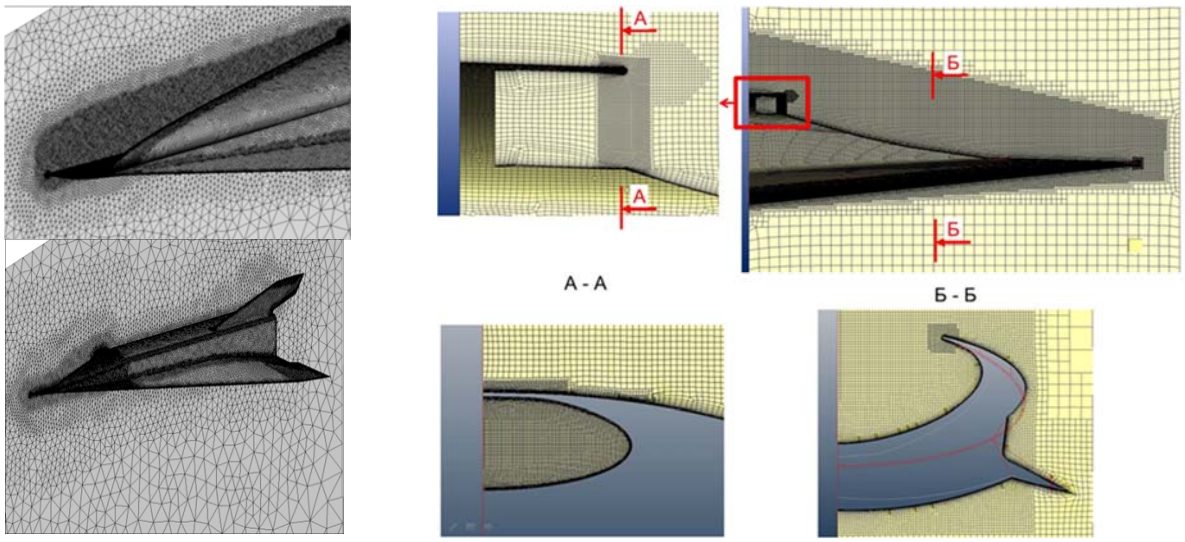


*Fig. 37: Numerical grids for ANSYS-FLUENT (left) and NUMECA (right).*

Flow field analyses show a peculiarity of a significant subsonic zone (represented by blue on pictures in Fig. 38), which occur in the air intake central part. The turbulent simulations have shown generally stable and regular flow in the air intake area.

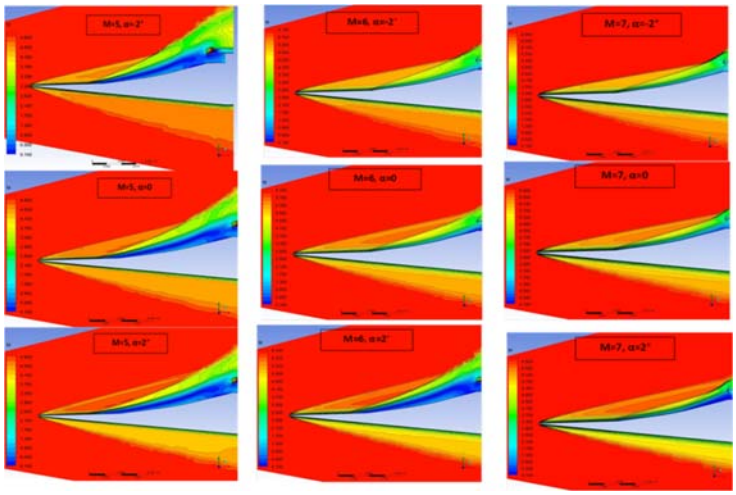

*Fig. 38: FLUENT results: Mach number fields in the intake symmetry plane, $M_\infty$=5, 6, 7; α=-2°, 0, 2°.*

In addition, high intake mass flow rate coefficients (f) throughout the considered range of Mach number and AoA were predicted, see Fig. 27.

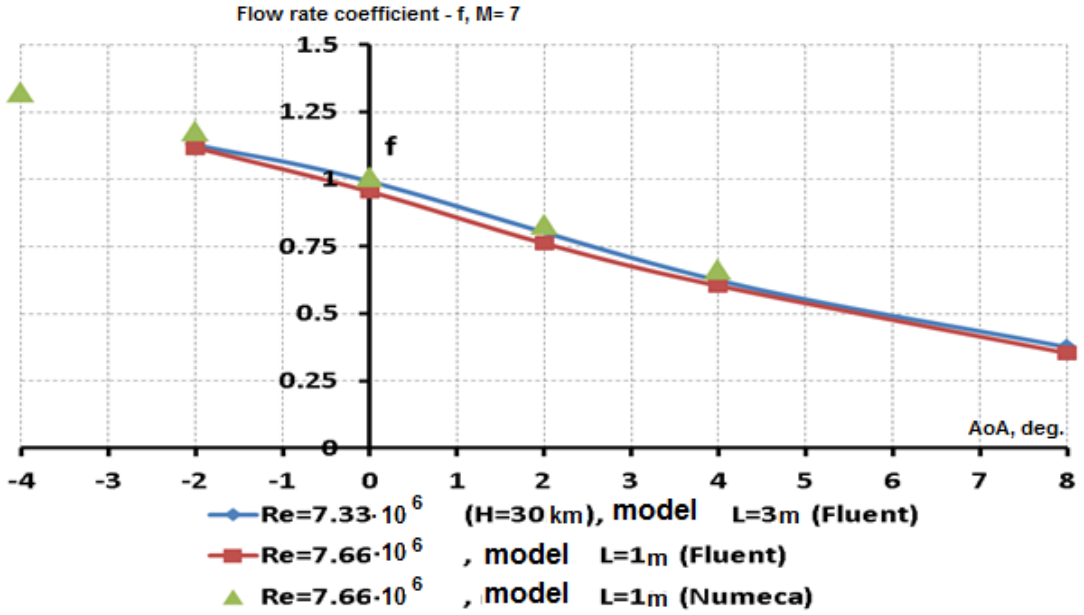


*Fig. 39: Comparison of ANSYS-FLUENT and NUMECA results: the intake mass flow rate coefficient, f vs. angle-of attack, AoA. $M_\infty$=7.*

The general trend is that the mass flow rate decreases monotonically with increasing AoA. It is important to note that when AoA=0 and Mach number is $M_\infty$= 7 or 8, the mass flow rate coefficient takes values close to 1, according to the results of both software packages ANSYS-FLUENT and NUMECA. At Mach $M_\infty$= 6, a sharp decrease of the mass flow rate was predicted in the range of AoA=0÷2° showing that the intake unstarts at positive AoA.
Comparison of the Mach number contours at the intake entrance section obtained by the two codes is presented in

Fig. 40. The results indicated a good agreement for basic parameters: intake mass flow rate coefficient, density, pressure and Mach number. As anticipated by the intake design requesting a turbulent boundary layer to cope with the compressive pressure gradient, laminar numerical simulations showed indeed the appearance of a separation zone which strongly effects the intake capture area at the combustor entrance and destroys its performance. This is clearly indicated in Fig. 41 showing the Mach number contours in the symmetry plane obtained by ANSYS-FLUENT with both laminar and turbulent BLs at $M_\infty$=7 and AoA=0. In the case of laminar flow, a large subsonic region is visible, which extends downstream and blocks almost the whole intake entrance area. In the case of turbulent BL, only a small local subsonic zone appears near the intake surface.

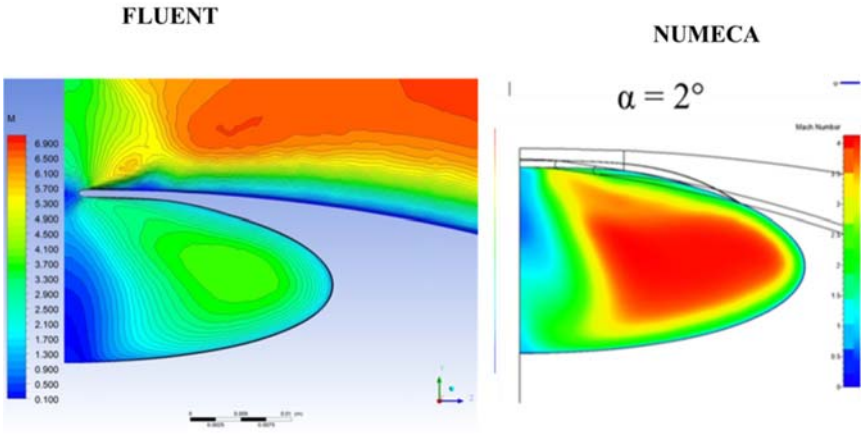


*Fig. 40: Comparison of ANSYS-FLUENT and NUMECA results: Mach number contours at the intake entrance section, $M_\infty$=7, α=2°.*

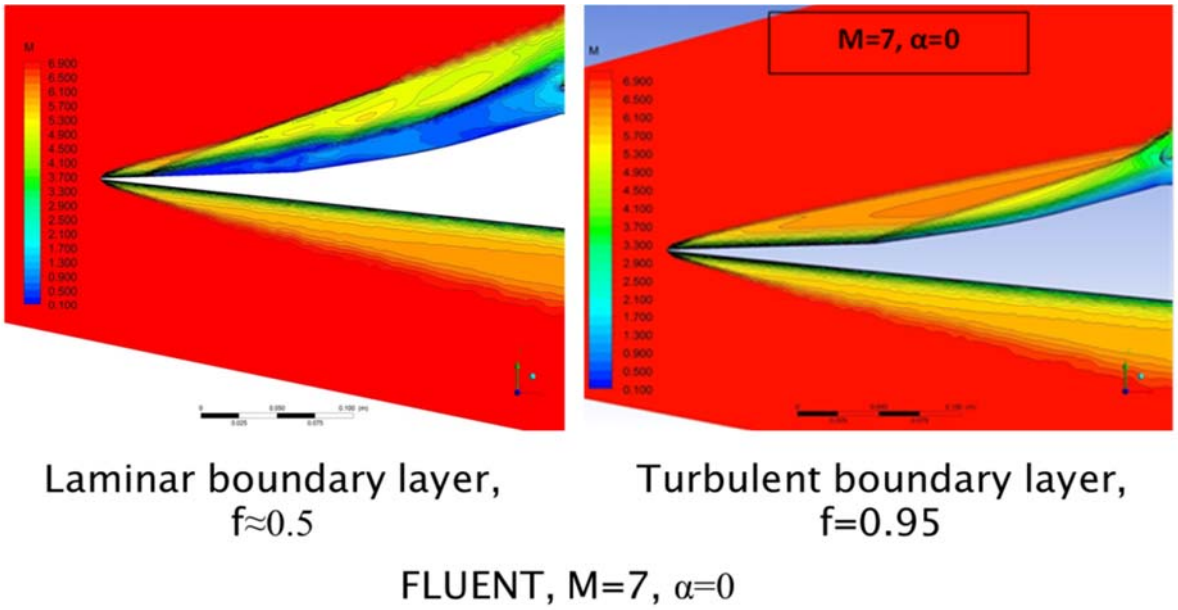


*Fig. 41: Mach number contours: ANSYS-FLUENT results with laminar (left) and turbulent (right) BLs.*

Comparisons of data on the intake mass flow rate coefficient extracted from numerical simulations (with preliminarily setting of turbulent and laminar BLs) and the experimental data obtained in the wind tunnel T-116 are shown in *Fig. 42*. Calculations with laminar BL gave significantly lower values of the intake mass flow rate coefficient f ≈ 0.5 ÷ 0.6. These results are much closer to the experimental data obtained on the model without BL tripping, which confirmed low mass flow rate coefficient and intake unstart at the most of test regimes due to the absence of a turbulent boundary layer on the intake.

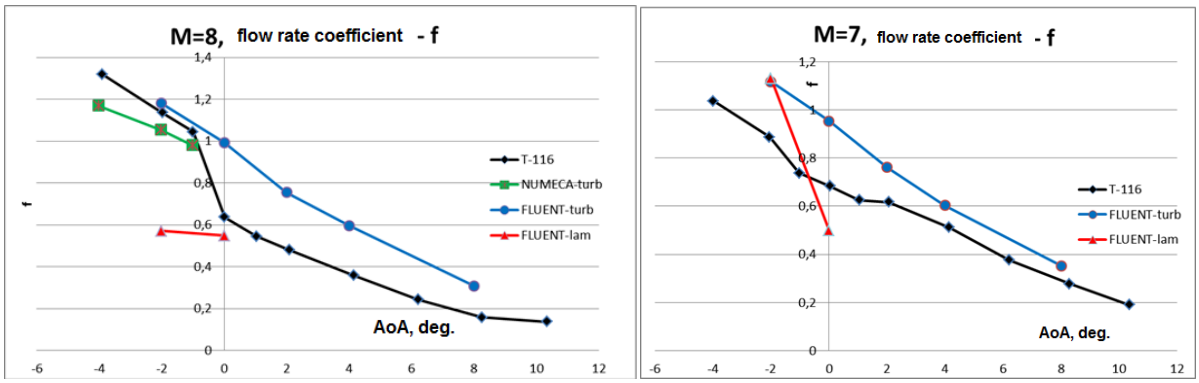


*Fig. 42: Comparison of ANSYS-FLUENT results (turbulent and laminar BLs) with the experimental data: the intake mass flow rate coefficient, f vs. angle-of-attack, AoA. $M_\infty$=8 and 7.*

### 1.3.3.2 Aerodynamic Tests on the Powered Configuration

TsAGI performed also experimental investigation in their supersonic and hypersonic wind tunnel T-116 to assess the aerodynamic performance on a 0.35 scaled the EFTV scramjet propelled concept. The approximately 1m long model with the internal flowpath allowed investigating the intake characteristics and taking into account the influence of the air passage through the engine propulsive path on the external aerodynamics of the vehicle (see Fig. 43). The model was tested at Mach numbers 6, 7 and 8.

The experimental results showed that the intake starting significantly depends on the BL state on the intake compression surface, i.e. laminar, transitional or turbulent. The first test series provided with ‘clean’ intake compression surface (without any BLT grit) showed that starting of the intake just appeared in a very limited range: at Mach 8 and negative AoA ≤ – 1°. At Mach number 7 and 6 the intake was unstarted.

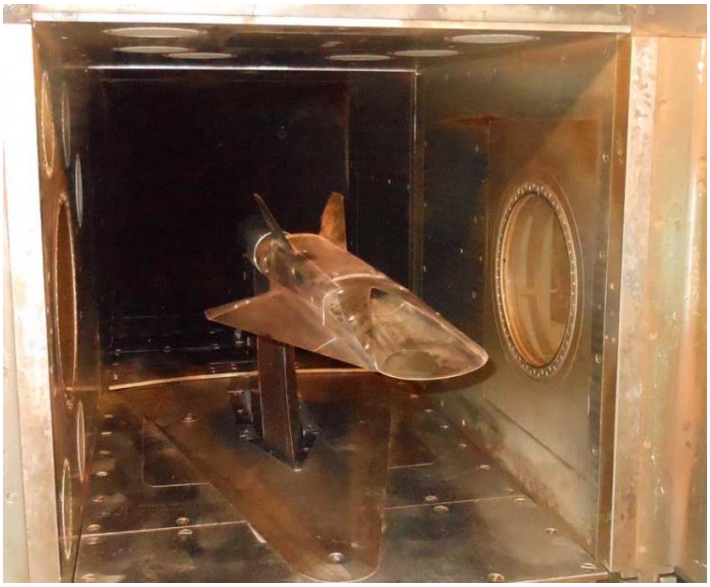

*Fig. 43: Aerodynamic model of the EFTV scramjet propelled option installed in the test section of TsAGI T-116 Wind Tunnel.*

A second test series was provided with different variants of transition grits, whose shapes are presented in Fig. 44. These included:

- 2 metallic strips with 3 rows of diamond-shaped roughness elements each; the heights of the roughness elements were 0.75mm and 1mm (var. 1),
- 10 screw heads of a 'dovetail' shape with height k=1.2mm and top diameter D = 3.8mm (var. 2),
- the same screw heads with wires of the diameter d = 0.5mm attached to the model surface by the screws in 'cross' position (var. 3) or
- in 'lines' position, i.e. parallel to the intake leading edge (var. 4).

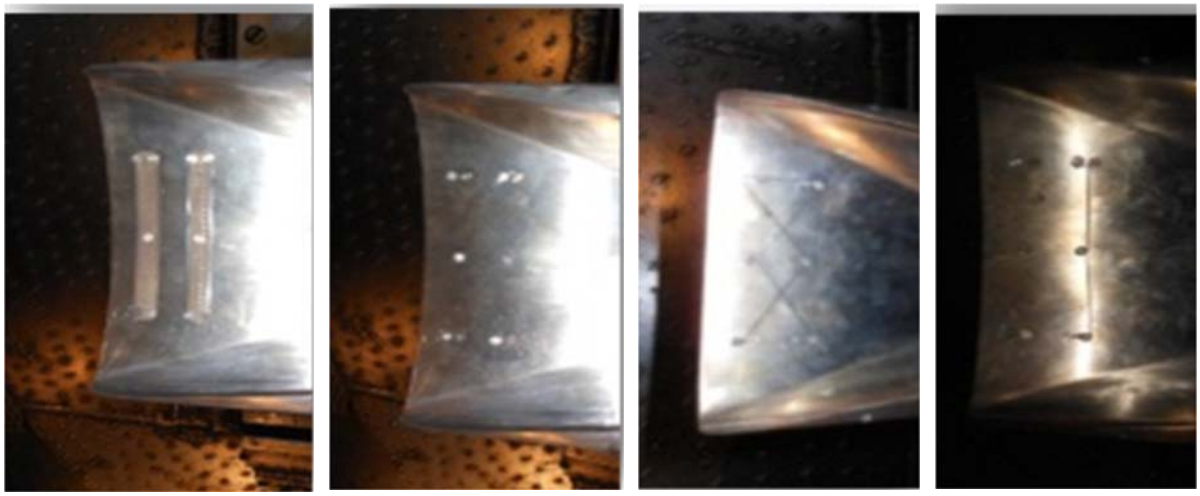


*Fig. 44: Different variants of the BLT grits used in the second test series.*

The tests showed that transition grit variant 1 did not improve the intake starting performance, while all the other variants from 2 to 4 led to significantly wider ranges of test conditions at which the intake was started. The main test results obtained at Mach numbers 8 and 7 in terms of the intake mass flow rate coefficient *f* are shown in Fig. 45. Low values of f (less than approximately 0.6) indicate the absence of the intake starting. These results were obtained, however, with widened intake throat area corresponding to a contraction ratio CR = 7.4 being lower than that of the original intake (CR = 8.6).

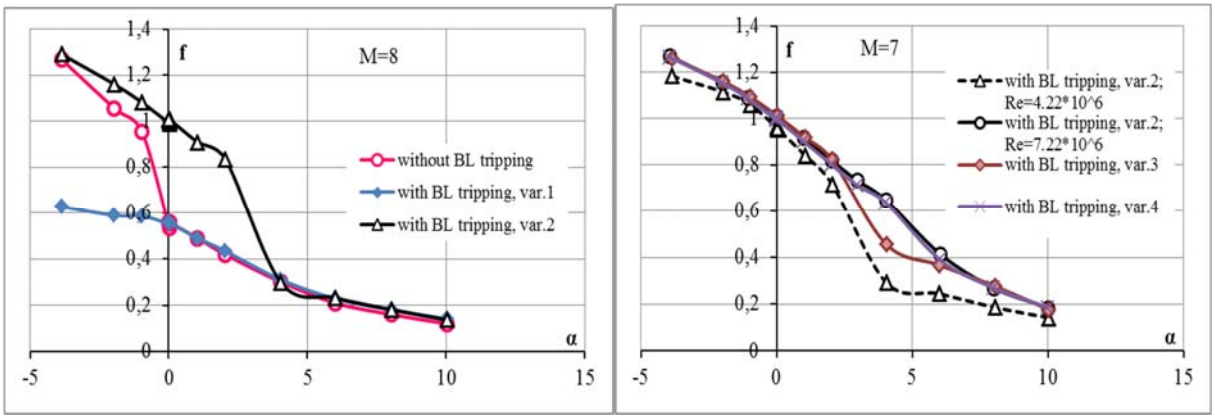


*Fig. 45: The intake mass flow rate coefficient f vs. angle-of-attack $\alpha$. Mach Numbers $M_\infty$ = 8 and 7.*

The external aerodynamics of the EFTV powered concept model was thoroughly investigated at Mach number 7. Its aerodynamic coefficients such as the drag force coefficient $C_D$, lift force coefficient $C_L$, aerodynamic efficiency $L/D$, and pitching moment coefficient $C_m$ vs. angle-of-attack of the model $\alpha$ at zero sideslip and different symmetrical flap deflections are presented in

Fig. 46. The reference parameters used for calculating the aerodynamic coefficients were the model plan-form area $S_{ref}$=0.2989m$^2$ and the model fuselage length measured from the leading edge of the intake to the base section $L_{ref}$=1.0066m. The moment reference centre MRC of the EFTV powered option model, similarly to that of the glider model, was located at 57% of the fuselage length.

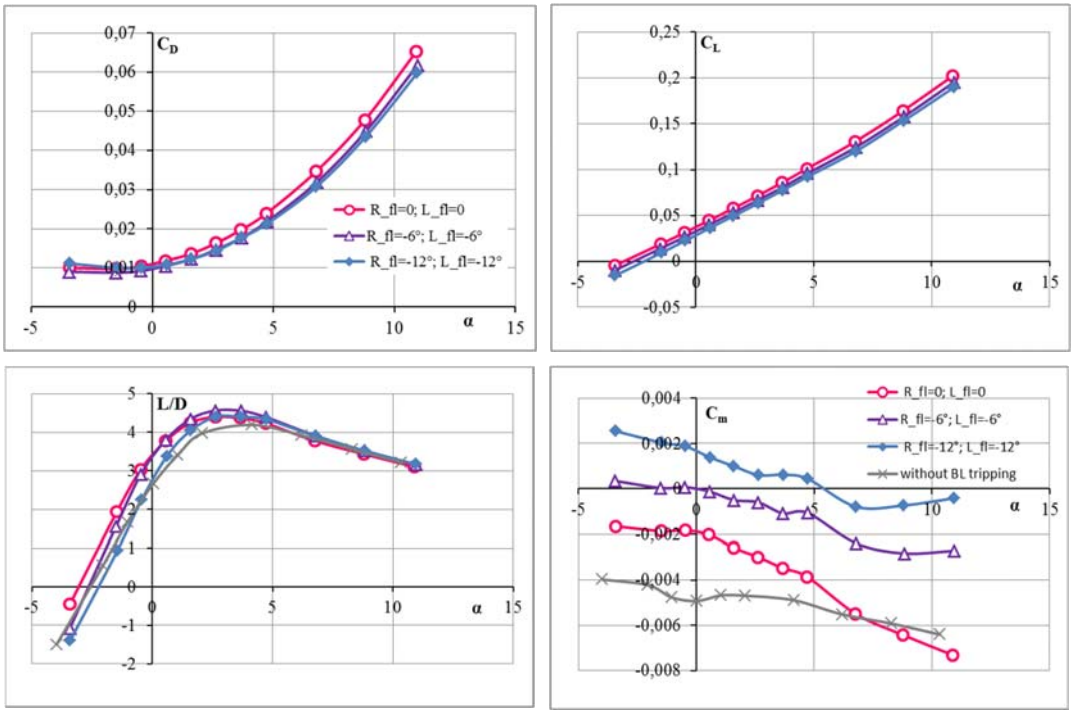


*Fig. 46: Drag and lift force coefficients, $C_D$ and $C_L$, aerodynamic efficiency, L/D and pitching moment coefficient, $C_m$ vs. angle-of attack, α. M = 7, transition grit variant 2 with different right (R_fl) and left (L_fl) flap deflection, and without transition grit, R_fl = L_fl = 0.*

It is seen that the maximum value of aerodynamic efficiency $(L/D)_{max}$ of the EFTV powered concept model with the transition grit variant 2 at $M$ = 7 is about 4.5, and the vehicle can easily be trimmed on pitch at angles-of-attack up to 5° with moderate flap deflections. The model without transition grit displays the value of $(L/D)_{max} \approx 4.1$, and its trimming on pitch becomes problematic within the considering range of flap deflection angles.

#### 1.3.3.3 Combustion Chamber Testing at the Connected Pipe Facility T-131 TsAGI

TsAGI also performed tests of the combustion chamber of the hydrogen-fuelled scramjet engine in the connected-pipe facility T-131. The model for these experimental tests was manufactured by CIAM, see Fig. 47. The main purpose of these experimental studies is to define the limits of stable operation of the combustion chamber. Beside this, it is also important to study the regimes at which self-ignition and flame stabilization are assured. The model with an elliptical combustion chamber is a full-scale model representing the actual size of the EFTV model. Such an approach makes it possible to conduct experimental investigations of the working principle without any adaptations. When mounted on the connected-pipe facility T-131, the combustion chamber is composed of eight separate sections interconnected through flanges (see Fig. 47): an intermediate part of the direct air heater, a part with critical section of the aerodynamic nozzle, supersonic part of the aerodynamic nozzle, a pre-injector section with two semi-struts, a section of combustion chamber with full-strut, a section of the 2D-nozzle and a section of the 3D-nozzle.

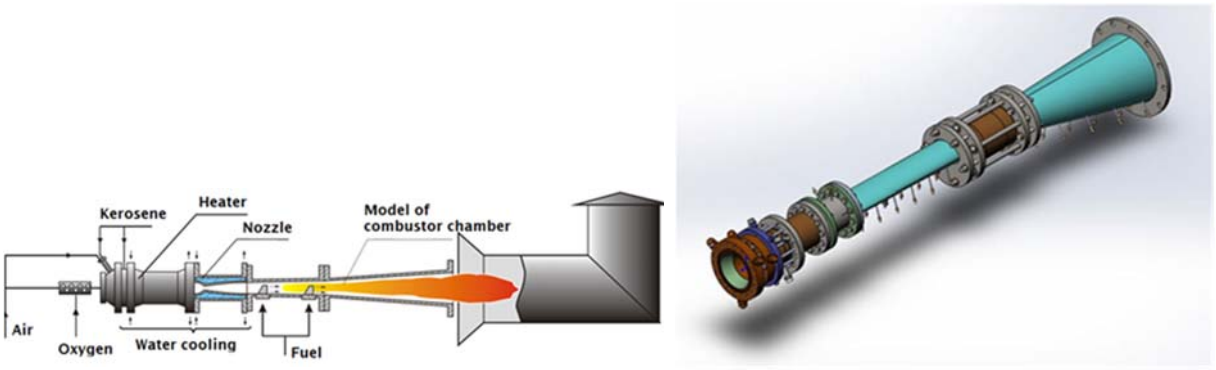


*Fig. 47: Scheme of the T-131 facility (left) and model of the hydrogen combustion chamber for testing (right).*

The T-131 facility (Fig. 47) is used mainly to study experimentally the operational process and the gas dynamics in ramjets and scramjets combustion chambers on the connected-pipe facility. The gas parameters in the air preheater of the test-bench allow simulating at the inlet of scramjet combustion chamber the total flow enthalpy, the M number and the pressure of flights in Mach number range 3÷10. Detailed description of the first test campaign can be found in [27].

During the first test series it was shown that the full-strut is located in the place with the maximum value of the static pressure in the model duct, which led to its burnout at parameters corresponding to the flight Mach number M = 7. Therefore, a new section was designed and manufactured in which the main fuel supply pylon was moved upstream as far as possible, based on the design limitations of the model (*Fig. 48*).

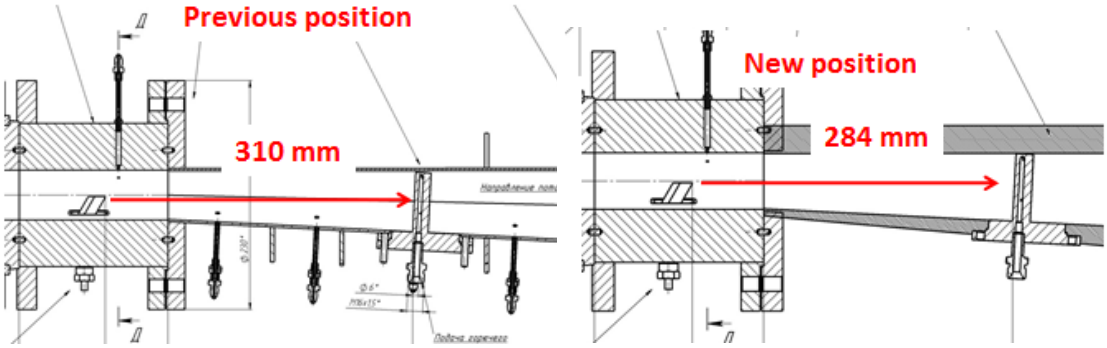


*Fig. 48: New full-strut position*

At the beginning of the test series, the runs were carried out with freestream conditions at the entrance of the model corresponding to the flight Mach number M = 6 with a fuel strategy similar to that in the previous series of tests (*Fig. 49*). In addition, tests were carried out with a larger amount of fuel (close to the maximum possible, without knocking the flow into the aerodynamic nozzle of the facility) fed into the model (ER = 0.85) through the full-strut (35%). It is shown that in the investigated regimes the maximum value of the static pressure occurs between the fuel supply rows, closer to the semi-struts. At these conditions, once more fuel is being supplied through the full-strut, the efficiency of the working process is increased. This indicates the need for fuel combustion in the expanding part of the model duct.

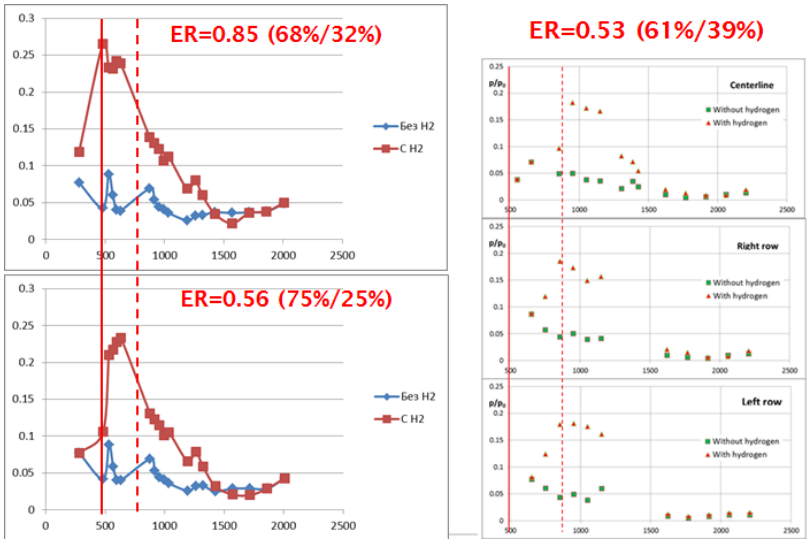


*Fig. 49: Results at conditions correspond to the flight Mach number M=6*

In several tests corresponding to a flight Mach = 7, the full-strut did not burn, which indicates a decrease in the thermal load on the strut and a displacement of the maximum value of the static pressure to the semi-struts. In the course of the tests, it was found that even at ER = 1.18, no knocking into the aerodynamic nozzle occurs, but even at ER = 0.74 the static pressure rise inside the model is insignificant (*Fig. 50*). It is shown that at ER = 1 it is necessary to supply more fuel through the full-strut, i.e. it is necessary to burn more fuel in a section with a constant cross section.

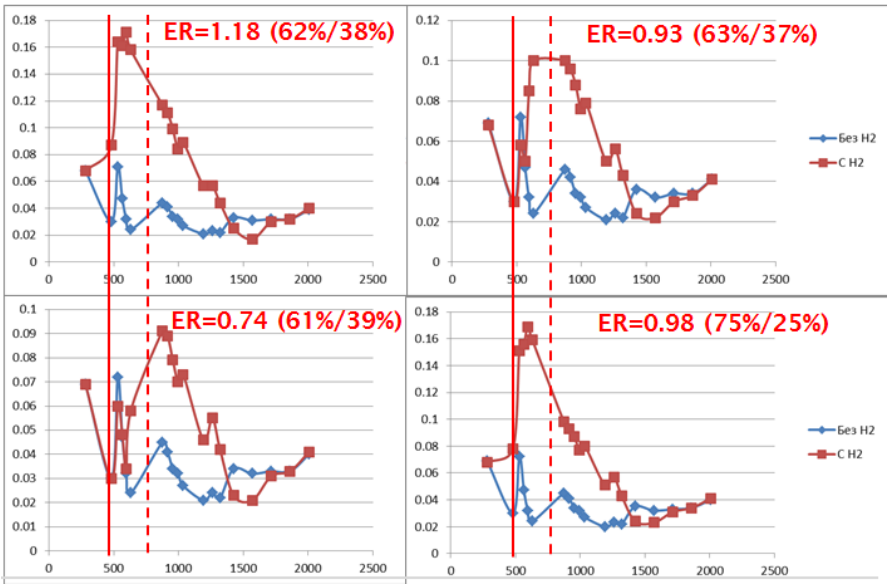


*Fig. 50: Results at conditions correspond to the flight Mach number M=7*

### 1.3.3.4 Propulsive Tests of the EFTV Powered Module in the CIAM Facility

Two different full-scale EFTV scramjet modules (Fig. 51 left) were designed and produced by CIAM for testing out in their free-jet ground test facility (*Fig. 52*). The purpose of these tests was the study of the operating conditions in the combustion chamber and the EFTV scramjet propelled option aero-propulsive balance demonstration [28]. The first model with simplified overall flowpath geometry [29] and having a low thermal inertia verified the principle operation of the scramjet module. It consisted of five main different parts: 1) air-intake with fuel pylon-injector; 2) combustion chamber; 3) nozzle; 4) frame; 5) power pylon. For the 2nd test, a scramjet model with a high-thermal heat sink capability was produced in CIAM (Fig. 51 right). The geometrical configuration of the combustion was made by an electro-erosive machine tool. The intake was milled out with

help of a 5-coordinate turning machine. The manufactured parts were melted to each other. The intake, combustion chamber and nozzle are equipped with pressure sensors and thermocouples for gasdynamic structure and combustion research.
Prior to the execution of the experimental campaign, a computational analysis was carried out to obtain the operating conditions for air-intake starting. A one-equation Spalart-Allmaras eddy viscosity model was used whereas the thermo-physical properties of the used gas are equal to fired heater combustion products properties. A sequence of numerical computations of EFTV scramjet module in the test bench [30] with conical nozzles were made. The nozzle accelerates the flow up to M=7.5. The air-intake was started during all investigated regimes (Fig. 53).

*Fig. 51: The full-scale EFTV scramjet module with low (left) and high thermal heat inertia (right).*

*Fig. 52: Low thermal heat inertia scramjet module installation in the CIAM free-jet facility.*

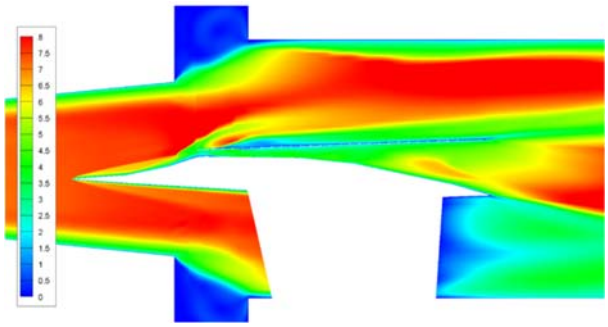

*Fig. 53: Mach number contours in the symmetry plane for EFTV module flow in CIAM facility conditions.*

The module was mounted on the thrust-measuring platform to determine the aero-propulsive balance. The main series of experiments was carried out with flow parameters corresponding to a flight altitude of the vehicle of $H_\infty$=33 km. Particular attention was paid to dependencies of scramjet thrust from the equivalence ratio (ER) and mass flow rate schedule among the struts. A total of 18 runs were carried out, with the total pressure and the total temperature of the oncoming flow being respectively p* = 6.1 - 6.5 MPa and T* = 2310 K. The experiments were carried out with the installation of the facility module at an angle of attack α = -2°. Dependences of the resulting longitudinal force coefficient $C_R$ on the angle of attack for different modes of engine operation are shown in *Fig. 55*.
The total force obtained in numerical simulation was compared with the experimental one, whose value with no fuel injection is -360 N. This 9% difference demonstrates an adequate accuracy of the calculation method.

During the tests, the equivalence ratio and the percentage of hydrogen flow through the fuel supply manifolds were varied. A total of 18 runs took place. During the runs the pressure in the vitiation heater was in the range $P_{vh}$ = 6.1 to 6.5 MPa, the temperature $T_{vh}$ = 2310 K. The modes and test results are shown in Table 3. The modes in which the positive aero-propulsive balance of the facility module was shown are bold. The positive aero-propulsive balance means that thrust generated by the engine, allowed exceeding the total aerodynamic drag of the facility model including support.

Table 3: Tests results

| Point number | $P_{vh}$, [Mpa] | ER | Fuel injection through bands % | Stable working process | Force [N] |
|---|---|---|---|---|---|
| 1 | 6.177 | 0.738 | 1/0 | + | -161.8 |
| 2 | 6.283 | 1.208 | 0.65/0.35 | + | -64.9 |
| 3 | 6.292 | 1.230 | 0.61/0.39 | + | -43.4 |
| 4 | 6.310 | 1.291 | 0.66/0.34 | + | -26.8 |
| 5 | 6.353 | 1.312 | 0.75/0.25 | + | -7.3 |
| 6 | 6.362 | 1.432 | 0.77/0.23 | - | -360.5 |
| 7 | 6.357 | 1.431 | 0.70/0.30 | - | -355.7 |
| **8** | **6.397** | **1.432** | **0.56/0.44** | **+** | **39.3** |
| **9** | **6.419** | **1.499** | **0.54/0.46** | **+** | **50.1** |
| **10** | **6.431** | **1.629** | **0.54/0.46** | **+** | **78.9** |
| 11 | 6.428 | 1.141 | 0.40/0.60 | - | -226.3 |
| 12 | 6.428 | 1.308 | 0.43/0.57 | - | -136.9 |
| **13** | **6.442** | **1.525** | **0.43/0.57** | **+** | **63.4** |
| **14** | **6.441** | **1.751** | **0.38/0.62** | **+** | **85.4** |
| 15 | 6.461 | 1.183 | 0.91/0.09 | - | -368.7 |
| 16 | 6.452 | 1.071 | 1/0 | - | -367.4 |
| 17 | 6.474 | 1.028 | 0.68/0.32 | + | -110.2 |
| 18 | 4.412 | 1.305 | 0.70/0.30 | - | -109.9 |

$P_{vh}$ – vitiation heater pressure,

ER – equivalence ratio,

Fuel injection through bands – percentage of fuel going through first/second fuel band,

Stable working process – means stable supersonic combustion in scramjet without thermal chocking,

Force – longitudinal force affected on facility module while fuel supplied

Positive aero-propulsive balance was demonstrated when the equivalence ratio ER was higher than 1.4. Effective thrust time history for ER=1.58 regime is shown in Fig. 54 (left). For combustion analysis, measured pressure distributions along the duct were obtained. On the right of Fig. 54, the pressure distributions with and without combustion are shown. High pressures in the duct in fuel supply case indicate clearly the presence of combustion, while the averaged flow is supersonic along the whole duct.

The blue lines on the graph of *Fig. 54* show the values of the numerically obtained external aerodynamic drag coefficients of the full vehicle (without taking into account the compression surface of the air intake device and the elements of the internal flow path). The black symbols show the values of the coefficient $C_R$, which were calculated at different coefficients ER = 0, 0.8, 1, 1.2. The red square and green triangle symbol are experimental points for ER = 1.0 and ER = 1.2 respectively. A positive aero-propulsive balance would lead to a negative $C_R$ value. As can be seen from all the cases considered, this condition is satisfied by the values of $C_R$ at the angle of attack α = -2 ° and ER = 0.8 and 1. However, once the same parameters are applied on the experimental values for the flowpath, it did not result in obtaining a positive aero-propulsion balance.

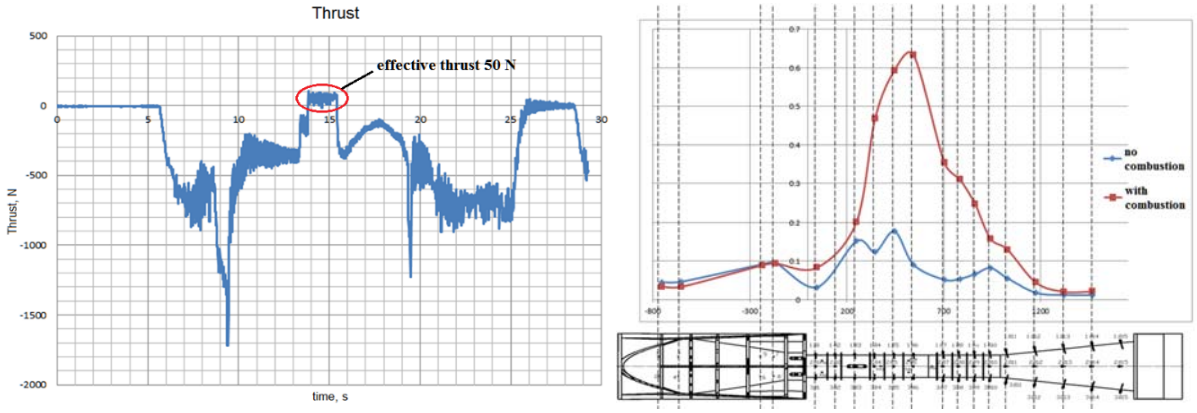


*Fig. 54: Effective thrust to time dependence (left) and Pressure distribution along the duct (right)*

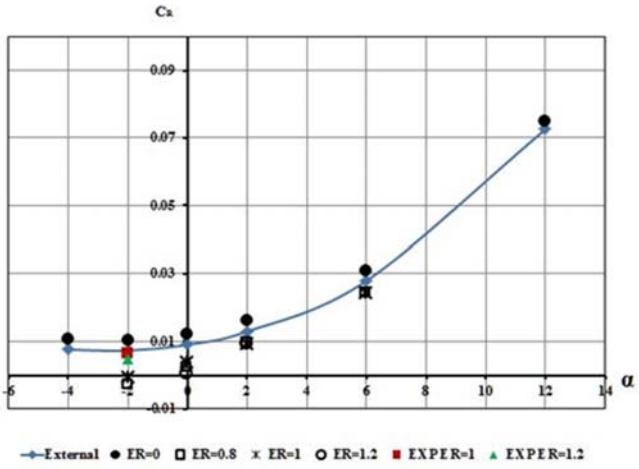


*Fig. 55: Numerical and experimental data of the EFTV powered concept model at M = 7 with scramjet operation: resulting force coefficient $C_R$*

In the experiments the values of the ER coefficient were varied which had a significant effect on the EFTV aero-propulsive balance. Fig. 56 shows the dependence of $C_R$ on ER. As can be seen from the graph with increasing ER, the value of the $C_R$ decreases due to the increase in thrust created by the engine. However, even at very high ER values, a positive aero-propulsive balance is not observed. The minimum value of the coefficient is $C_R$ = 0.00267 at ER = 1.629 [31]. It should be noted that this value of $C_R$ is relatively small and close to aero-propulsive balance [28]. It was shown earlier that the combustion efficiency in the experiments did not exceed η = 0.6 at the maximum ER. Even a slight increase of the combustion efficiency due to an improvement in the quality of the working process in the combustion chamber will lead to a positive aero-propulsive balance of EFTV. Hence, it can be said that the proposed configuration is capable of providing a positive aero-propulsive balance. This will be the major objective with the high-thermal resource model during the 2nd test campaign.

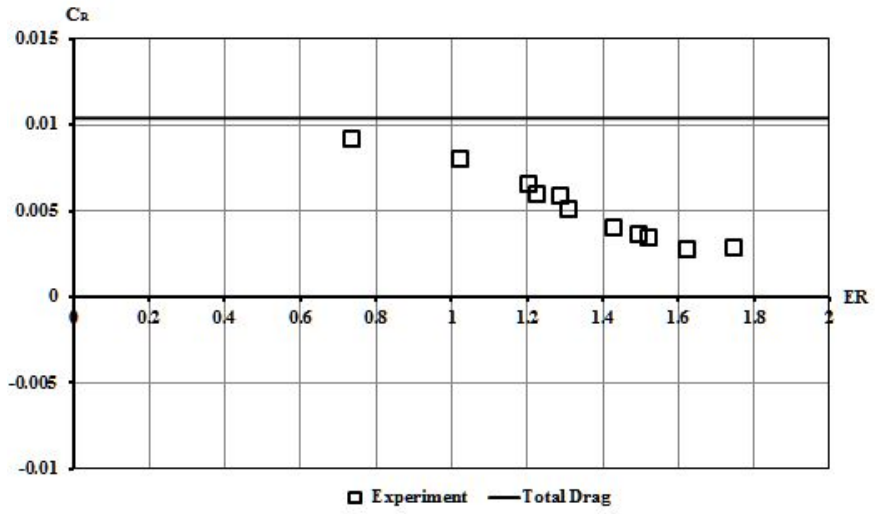


*Fig. 56: Experimental resulting force coefficient $C_R$ of the EFTV powered concept at M = 7with scramjet operation*

### 1.3.3.5 Flight Control

A preliminary EFTV propelled flight trajectory was built by LII based upon estimates of aero-propulsive characteristics provided by TsAGI and CIAM, ensuring the achievement of scientific goals and satisfying the flight experiment constraints (Fig. 57).

The main purpose of this flight experiment is to study the engine subject to the constraints of 27 km <H <32 km, 7 <M <8 at a flight path angle $\gamma$ close to zero. In the course of preliminary studies, it was shown that after the ESM separation the EFTV insertion into the engine research window is possible. However the model flight trajectory passes near the lower boundary of the research window both with respect to the M number and the flight altitude H. Maximization of the M number of the EFTV insertion into the engine research window resulted in the decrease of the insertion altitude and vice versa. Maximizing the altitude of the EFTV insertion into the engine research window resulted in a decrease of the insertion M number. Therefore, to cope with the problem of the trajectory selection, also the segment of the pull-out manoeuvre was considered in the optimization formulation in order to maximize the altitude of the EFTV insertion into the engine research window [27].

The optimized program α(t) applied in the EFTV longitudinal motion modelling, with due regard for the chosen algorithm of the automatic control system operation, allowed the EFTV to be inserted into the engine research window with parameters: M = 7.0, H = 27 900 m. In the engine research window at M=7 the EFTV flight takes place without loss of the M number and flight path angle; the selected parameters of the autopilot provide the EFTV stabilization at the preset AoA =-0.5$^0$ after the engine start in less than 0.25 seconds.

After the engine is turned off, the further flight of the EFTV is carried out with a bank angle $\Phi$ of 40$^0$, which provides the necessary conditions for the telemetry data reception by ground TM stations throughout the entire flight of the EFTV. In this case, the idea is to apply a sinusoid perturbation on the angle of attack of the EFTV in the vicinity of the a priori estimate of the angle of attack $\alpha_{max}$(M), corresponding to the maximum aerodynamic efficiency of the vehicle. It is expected that such an imposed perturbation will make it possible to refine the estimate of $\alpha_{max}$(M) by the results of the flight experiment in the range of M numbers from 7 to 2.

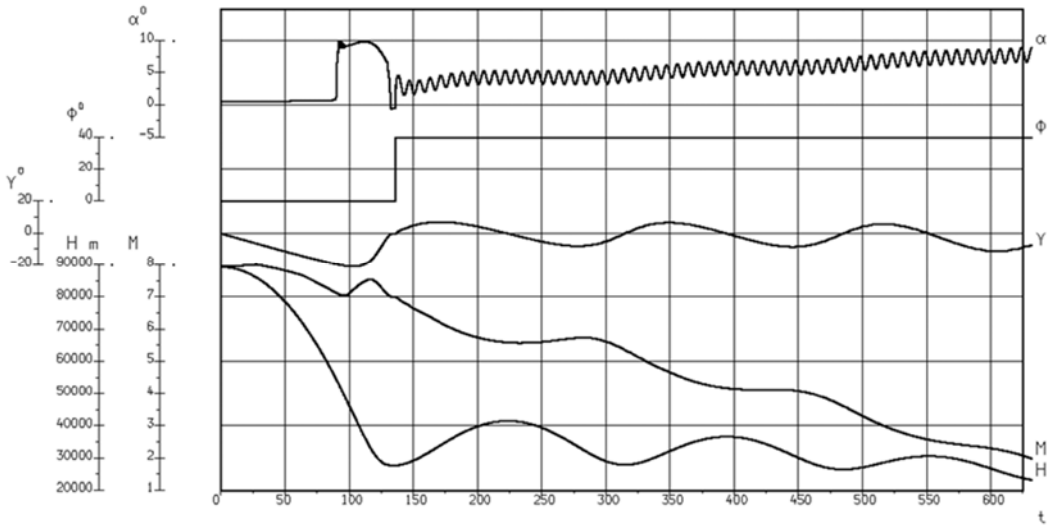


*Fig. 57: Preliminary flight trajectory of the propelled EFTV*

### 1.3.4 Booster Configuration

The VS-50 vehicle is based on the 1.46 m diameter thrust vector controlled S50 rocket motor with 12 tons solid propellant and a 1.0 m diameter S44 upper stage with 0.8 tons solid propellant. Since this vehicle overshoots the performance requirements of the Hexafly-INT flight mission, it was decided to utilize the VS-50 as a single-stage version without the S44 upper stage. By adapting the Launch Vehicle Service Module structure, the single-stage VS-50 with Hexafly-Int payload can be flown with the same fairing and similar control authority as the two-stage VS-50 without any further adaptions (see *Fig. 58*).

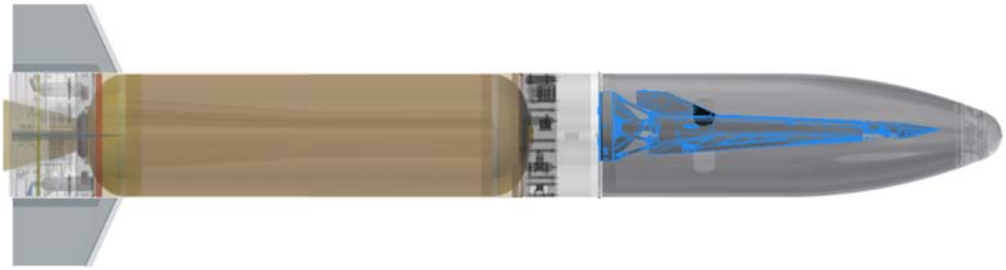

*Fig. 58: VS-50 single-stage with Hexafly-INT payload*

The VS-50 vehicle development is a joint project of DCTA and DLR, started in 2015. DCTA is responsible for the S50 motor development and forward module. DLR is in charge for the thrust vector assembly (TVA), fin assembly, interstage adapter, service module, clamp band joints, fairing and GNC. The S50 motor successfully completed a burst test in 11/2018 (see *Fig. 59*) and passed CDR in 05/2019. Structural tests were successfully completed in 08/2019 and two static firing tests including the thrust vector system provided by DLR are scheduled next. The TVA (see *Fig. 60*) passed CDR in 12/2018 and successfully completed HiL (Hardware in the Loop)-Tests in 10/2019 as well as vibration and acoustic qualification tests in 11/2019.

To build up a lightweight RF transparent Fairing for the VS-50 Rocket carbon fibers are not applicable. Therefore, glass fiber was chosen using an HT epoxy matrix (Tg > 130°C). To gain the needed stiffness (buckling) while remaining a smooth inner and outer surface, the design is based on a sandwich structure. As the overall dimension is more than 4m in length and 1.5m in diameter, the use of a single piece production combined in one step is not reasonable. Two hatches (positioned symmetrically in 180°) are needed for having access to the payload or other elements below the fairing. Therefore, a production in 2 half shells or 4 quarter shells would fit to the geometry. The quarter shells were chosen for two main reasons: first the accessibility to an autoclave and second: the easier (and therefore more reliable) layup. The layup at smaller parts are evidently faster. This gives a longer handling time of each layer (related to the pot-life of the resin).
To get the stiffness of a mold of this size an over-dimensioned standard steel-truss structure was chosen. On this structure the standard mold-material was glued and milled to the original shape (*Fig. 61*).

*Fig. 59: S50 motor case burst test at AviBras*

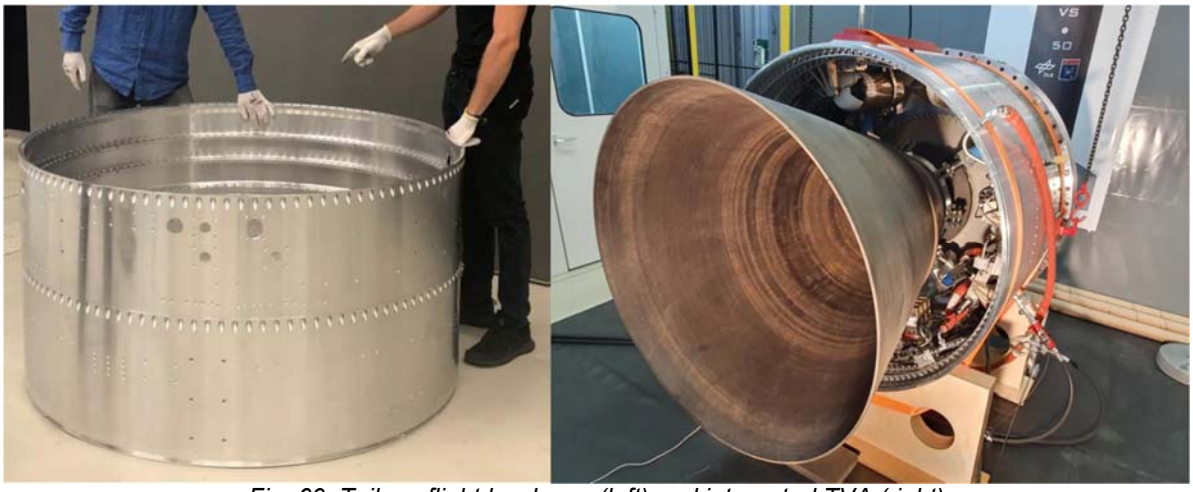

*Fig. 60: Tailcan flight hardware (left) and integrated TVA (right)*

*Fig. 61: Fairing mold after milling (left) and GFK lay-up of access hole (right)*

### 1.3.5 Conclusions

The development status on a high-speed glider and a propelled concept at both low and high-speed were described.

The overall layout of the glider vehicle was generally discussed. The feasibility of a flight experiment for a glider concept in all its aspects was assessed based on numerical results and windtunnel campaigns. The use of a sounding rocket, a release at an apogee of 90km followed by a pull-out manoeuvre allows flight-testing the glider at Mach 7-8 at a flight altitude of about 30km.

The low-speed vehicle concept has shown both numerically and experimentally to have the necessary control authority. The selected electrical engine for the remote controlled vehicle can provide enough thrust during take-off and assure the feasibility of the low-speed flight tests in Australia.

The aero-propulsive performance of the propelled concept was also investigated numerically and experimentally. The outcome of the study indicated a positive thrust generation during the experiments at these high speeds but still needs to be proven for the fully equipped vehicle. The intake was shown to be sensitive to the transition location and needs to be triggered on the small scale to assure a representative flow field as originally designed.

## 1.4 Potential Impact and Use

### 1.4.1 Expected impacts listed in the work programme

#### 1.4.1.1 Expected impact for International Cooperation on Civil High Speed Air Transport Research

Independent of technological feasibilities, high-speed transportation will only be considered worthwhile for global deployment if its overall performance is promising. This is entirely dictated by the range potential and the fuel consumption which depend largely on the cruise efficiency of the vehicle. If this potential cannot be demonstrated in flight, a breakthrough or a radical change will never be realized. It is essential to progress beyond the demonstration of core principals. It is important to take the opportunity utilizing high-speed flight experiments within the atmosphere to proof global performance of promising radically new concepts which have all elements available to cause a step change in aeronautics and air transport in the 2nd half of this century. The outcome of the present activity will provide the much more needed global performance demonstration for high-speed transportation at a lower cost than e.g. in the USA. Though (costly) technology demonstrators are very valuable, they have a lower relevance to the served purpose if the global performance cannot be reached or demonstrated.

The past and presently on-going projects *ATLLAS I/II* and *LAPCAT I/II* each address particular disciplines and technologies required to achieve long range flights at high speed. The outcome of each of these projects demonstrated already the technical viability and practicability (or feasibility) of long-range flights at high speed. The statement is underpinned by simulations and ground-experiments indicating that materials, engines, vehicle concepts, aerodynamics, integration issues are yet fully explored and tested on-ground. The researchers and engineers are now hampered by the limitations of the ground facilities as it is not possible to proceed beyond the present scale and integration level. Also numerical simulations need to be validated beyond the limitations of the ground-facilities allowing a proper extrapolation towards the envisaged scales.

Creating the grounds for a flight experiment is a first crucial step to overcome the above mentioned limitations. The *HEXAFLY* project already highlighted which of the different launch platforms and payload sizes is technically and financially feasible while still being challenging as a high-speed flight experiment. Along with elaborated ROM-costs, this has an important impact on the layout of roadmaps for high-speed vehicles within Europe. Further, a preliminary layout of a high-speed experimental vehicle is already elaborated and paves the way for a proper definition of an international flight project coordinated by Europe where key points of high-speed flight will be addressed. For civil high-speed transportation, this could then be marked as an “unique” and a “first” on an international level since the bilateral cooperation between the UK and France leading towards the Concorde.

The credibility to realize this flight is largely based upon the experience and know-how gathered by the main European partners CIRA (*USV, SHARK*) and DLR (*SHEFEX I/II*) with the recent supersonic and hypersonic flight experiments. These flight projects involved the complete development line like the layout of the scientific payload, the on-ground experimental campaigns and the detailed design of the vehicle including all needed (sub)systems, the assembly, integration, testing and verification. A similar process was conducted in parallel starting off with the selection and trade-offs of launch platforms and launch ranges. Here, the mutual impact on the scientific payload and finally the flight execution itself and flight data extraction were assessed. Special attention should be drawn to the large and globally recognized experience of the launch provider DLR-Moraba. Being involved in setting up the appropriate launch platforms for a wide variety of these unusual or non-classical hypersonic flight experiments worldwide, is an important element to establish the proposed flight test.

However, the project ambition goes well beyond the scientific goals of the experimental flight tests mentioned above. The challenges projected here are related to a sustained, powered flight of a vehicle with a high lifting potential at high speed. Having propulsion on-board significantly increases the complexity as apart from the aerodynamic balance also the aero-propulsive balance has to be taken into account. Moreover, the heating of the structure is not any longer limited to the external skin, but is now also generated all along the internal flowpath from intake to nozzle exit. Here the temperatures inside the core of the vehicle are by far higher than the external heat loads. This needs to be properly mastered and designed.

To mitigate this risk and cross-check the viability of the design prior to flight testing, a ground-test would be ideal at full scale. However, very limited on-ground facilities exist worldwide which could perform these kind of tests. Among the partners, potential facilities are the S4 at ONERA in France and the C16VK at CIAM in Russia.

Other risk-mitigating measures are foreseen to assure the success of the flight, i.e. separation issues, flight controllability, detailed analysis and cross-check with various high-fidelity tools, etc. These elements can and

will be handled by more than one partner both on European and on international side. Hence the present consortium certainly has the critical mass and technical potential to make this flight to conduct a successful flight.

Apart from this, the financial contribution both from the EC and the international partners is crucial to realize this flight experiment. Luckily, the long lead time to set up this proposal along with the on-going feasibility studies of *HEXAFLY* in parallel have allowed the team to verify and trade-off various flight concepts along with the related ROM costs. This pre-study gave the partners enough confidence to raise their in-kind contribution assuring the project can be realized with the planned financial means provided the project is evolving as planned.

Since the start, all international partners in the consortium were very keen to take part and realize this challenging project, realizing that each of them have a dedicated responsibility and need to share both their technical and financial means to set-up and realize this project. The technical exchange will occur at different levels:

- Provision of designs and layouts
- Provision of hardware components and (sub)systems to build the scientific payload
- Joint assembly and integration of all systems into the complete payload
- Providing access to unique facilities in terms of size and cost
- Provision of expertise in flight preparation and execution

The exchange of this sensitive information during the preparation of the proposal has already created durable links between the European and international partners. This will be further enhanced once the project will be kicked-off.

#### 1.4.1.2 Expected impact for Pioneering the Air Transport of the Future

The projected impact for the activity 7.1.6. is formulated in the Work Programme [9] as '*exploring more radical, environmentally efficient, accessible and innovative technologies that might facilitate the step change required for air transport in the second half of this century and beyond*'. Within the activity 'Pioneering the Air Transport of the Future', the proposal should investigate step changes in aeronautics and air transport such as new propulsion and lifting concepts, new methods of aircraft control etc...

The present project is fully in line with these impact expectations as it investigates new approaches to create propulsion power and novel aircraft configurations for future high-speed air transportation concepts. At the same time it will explore the application of hydrogen as a renewable energy source while addressing as well the environmental concerns.

Supersonic aircrafts propelled by airbreathing engines require a particular shape and size as well as a harmonized aircraft/engine integration in order to achieve an operational vehicle. Intake, combustion chamber and nozzle do form an intrinsic part of the complete aircraft. The forebody serves already as a part of the intake whereas the aftbody forms a part of the exit nozzle. The shape and size of these components largely determine the optimal functioning of the engine and improve the total drag of the vehicle. This observation was carefully addressed within LAPCAT I/II resulting in a dorsal mounted engine nicely blended into a waverider shape on the windward side. By this approach, a large internal volume could be realized while retaining the high aerodynamic performance of a waverider. The inward turning duct and the surface/volume efficient combustor allowed further improving the overall propulsive and cruising efficiency.

The development of some of the basic technologies to prove the feasibility of high-speed vehicles as well as the related flight experiment has been initiated in the previous projects ATLLAS I/II, LAPCAT I/II and HEXAFLY. All of these projects have been funded by this activity *'pioneering the air transport of the future'*. This will be pursued with the present project but now at an international level with extension towards a complete design of a flight-worthy high-speed experimental vehicle will be realized.

The proposed vehicle concept will enable to prove a combination of technical breakthroughs with respect to aerodynamic, propulsion and material efficiency. Its aspired higher cruise potential will then experimentally be demonstrated and will bring up a radical new approach to high-speed vehicles and consequently also to advanced propulsion technologies and the energy needed for flight.

Finally, this vehicle will be a landmark and form a cornerstone to investigate the credibility of the numerical tools and the ground-based facilities for all partners involved. The actual flight is the logical next step towards the prediction of the aero-propulsive balance and the validation of the numerical tools and on-ground facilities.

#### 1.4.1.3 Expected impact for the greening of air transport

Apart from the exploration of new approaches to create propulsion power and novel aircraft configurations for future high-speed air transportation concepts, the application of hydrogen as a renewable energy source will be simultaneously explored addressing as well the environmental concerns.

The latter is also a major concern of the Activity 7.1.1 on 'The Greening of Air Transport'. The expected impact formulated in the Work Programme is:

a. reduction of $CO_2$ emissions by 50% per passenger-kilometre
b. reduction of $NO_x$ emission by 80% in landing and take-off according to ICAO standards and won to 5g/kg of fuel burnt in cruise
c. reduction of unburned hydrocarbons and CO emission by 50% according to ICAO standards

The use of hydrogen as the basic fuel for the conceptual studies and the experiments will ensure the envisaged reduction of $CO_2$, CO and unburned hydrocarbons emissions. Special attention is drawn to the reduction of $NO_x$ by using advanced combustor and injector systems as well as the fuel consumption.

Cleaner engines

A major part ofproject is related to the understanding and improvement of the combustion physics for airbreathing engines at high speed. Hydrogen is considered as an alternative fuel. Since hydrogen has the largest amount of heat per unit weight and can sustain ignition and combustion at strain rates much greater than those of gaseous hydrocarbon (HC), it was shown to be the best fuel for the application in mind; furthermore its low molecular weight favours high specific impulse and hence high propulsion efficiency. It goes without saying that water, the resulting combustion product, is the cleanest form of emission that one can imagine. Its major drawback is its low energy density implying large and bulky fuel tanks. A part of *LAPCAT-II* focused on different injector strategies and combustor shapes lowering the emissions mainly due to increased thermodynamic efficiency and lower fuel consumption...

Finally, a considerable portion of the project will also look into engine/airframe integration inevitable to reduce the total drag. Intakes, combustion chambers and nozzle exits need to be tuned to each other to work optimally in all conditions. This is mainly achieved by experimental and numerical fluid dynamics. The investigation includes also the reduction of flow unsteadiness coming from the high-speed intakes, combustion chambers and nozzles and which are also responsible for a considerable part of the drag. As a consequence, all measures to drag reduction will effectively lead to lower fuel consumption and hence into lower emissions.

Decrease of noise emission

A particular case of noise emission for high speed transportation is linked to sonic boom. The intensity is actually proportional to the square of the overpressure, so when the peak pressure decreases the sonic boom loudness reduces. In parallel it has been established that extension of the rise time decreases the component of high frequency which is more severe for human sense of hearing compared to low frequency. During the *ATLLAS-I & II* studies, sound levels for a Mach 6 vehicle were predicted to be of the same order as the ones generated by the Concorde. This was however based upon a turbulence-free atmosphere which has an attenuating effect particularly for high altitude flights. As the envisaged vehicle aims for altitudes above 24km, an important decrease in sound level and/or increase in time rise might be obtained.

Dedicated sonic boom measurements will be performed in a 200m long ballistic range facility allowing to mimic different flight conditions such as speeds, altitudes… to assess not only the effect of the vehicle shape but also the propagation of the perturbations in the vicinity of the vehicle i.e. within O(10) vehicle lengths . This would provide valuable sonic perturbation data otherwise not measurable and providing validation data for the applied numerical tools allowing then a vehicle shape optimization.

#### 1.4.1.4 Overall Expected Impact

In terms of **overall expected impact** identified in the work programme for all areas and topics, the project is fully in line with the listed points:

1. *Reduction of greenhouse gases emission, particularly $CO_2$ and pollutants*
   A major objective of *HEXAFLY-INT* is related to flight test the improvement of the combustion physics for airbreathing engines at high speed. Since the alternative fuel hydrogen has the largest amount of heat per unit weight, it was shown to be the best fuel for the application in mind. Furthermore its low molecular weight favours high specific impulse and hence high propulsion efficiency. It goes without saying that

water, the resulting combustion product, is the cleanest form of emission that one can imagine. There is no release of CO2, unburned hydrocarbons (UHC) or other particles along its entire flight trajectory. Its major drawback is its low energy density implying large and bulky fuel tanks. However, when properly conceived this could be used in favour of lower wing loadings and hence alleviate the sonic boom impact. Within LAPCAT II, it was shown so far that NOx-emission during cruise could be lower or similar to the goal of 5g/kg fuel set as objective by the EC.
Finally, the project enables to check the engine/airframe integration optimization done within *LAPCAT II*, enabling a total drag reduction. Intakes, combustion chambers and nozzle exits need to be tuned to each other to work optimally in all conditions. The investigation includes also the reduction of flow unsteadiness coming from the high-speed intakes, combustion chambers and nozzles and which are also responsible for a considerable part of the drag. As a consequence, all measures to drag reduction will effectively lead to lower fuel consumption and hence into lower emissions.

2. *Increase of safety*
   There is a strong connection of *HEXAFLY-INT* with the improvement of aircraft safety with respect to high-speed vehicles. One of the objectives is to prevent the unsteadiness in intakes, combustion chambers and nozzles. Such unsteadiness is the source of aerodynamic loads for the structure, leading to the fatigue of materials. An improvement of this point will lead to structures working in better conditions, minimizing the risk of mechanical damage, minimizing the necessity of maintenance, and finally safer and cost-effective systems.
3. *Easy mobility of passenger and goods*
   With the present class of aircraft, long-distance flights still require a long and exhaustive stay on the aircraft to reach the final destination. This has not only a negative impact on the passenger's comfort but clearly also on the economics and the efficient use of both human and infrastructural resources. Decreasing the actual flight time by a factor of 3 to 5 will clearly improve this situation: less time lost on the long-haul routes, faster delivery of time-critical goods and more intensive use of the aircrafts. This will result into a broader choice of available transport means to reach the final destination.
4. *Higher Competitiveness of the European Transport Industry*
   The work proposed by *HEXAFLY-INT* strives for appropriately positioning Europe in the world-wide efforts to propel air vehicles to higher speeds routinely in a reliable and safe way. These efforts are largest in the US, based on a 40-year long heritage and costly flight experimentations, but exist also in Russia, Australia and Japan and to some extent in Europe. It is clear that currently the major impetus comes from its potential military use. It is, however, also clear that once the technology is sufficiently mastered for military application, the corresponding industries will apply their knowledge also to the design of civil high-speed commercial transport vehicles. Europe needs to prepare for this long-term situation.
   Individual member states of the EU cannot afford the same financial investigation and impact as the US. In order to accomplish international collaborations, we have to accelerate our research and demonstrate our efforts now on European level. Unless Europe reacts and accelerates research and development efforts now, it runs great risk to allow, in particular, the USA to obtain a certain monopoly and control with respect to very high speed transport. On the other hand, Europe needs to become a global leader or at least a very well educated partner if it wants to exercise influence in a global partnership framework. It should be clear that such transport systems cannot be accomplished by one single country. *HEXAFLY-INT* can be seen as a catalyst for future international collaboration and funding.
   Beneficial for European industry are the requirements of the envisaged product. Since the goal cannot be achieved by simply applying conventional technologies, striving for success results in innovative thinking, concepts and developments, closely linked to new analytical and computational as well as experimental approaches and tools. Thus, industries and research organisations will move to or stay at the leading edge of development capabilities, which is beneficial by itself for capabilities with respect to competitiveness potential.
5. *Demonstration, Validation and Testing*
   *HEXAFLY-INT* will contribute in enhancing the predictive capability of CFD methods currently used by the Aeronautical industry. Advanced physical insight will yield to efficient modelling techniques for system studies, subsonic low-pressure and supersonic combustion and aerodynamic unsteadiness related to high-speed aerodynamic flows within the different parts of the engine. Especially the unique data-base (numerical, experimental and flight), to be constituted by the present project, will contribute to a better physical comprehension of the particular combustion effects and of the unsteadiness of aerodynamic devices for high-speed flows vehicle design. The experimental database will be obtained from advanced experimental methods, for high-speed unsteady chemically reactive, compressible flows experienced in advanced airbreathing engines. These data, together with the complex turbulence-combustion models will be widely used for validation purposes. Further, the advanced CFD methods resulting from *LAPCAT-*

*I* and *LAPCAT-II* including detailed flow models for external and internal aerothermodynamics will be applied for the nose-to-tail investigations of the experimental flight vehicle configuration. This achievement will contribute to an added value in advanced propulsion design and therefore in increased modelling and simulation capabilities of the European industry and institutes.

### Steps needed to bring about these impacts

The largest challenge to be realized is to combine all the different technologies into a flight vehicle concept. The project is performed stepwise from a preliminary definition originating from HEXAFLY up to a detailed design, the manufacturing process and finally the assembly. Following this approach the probability to detect the major problems well ahead in time to adapt and to secure the final goal is very high. The most obvious and direct step to realize the first major impact is the realization of a flight experiment realizing the outcome of HEXAFLY: demonstrating an optimal cruise potential for a high-speed cruise vehicle in a controlled way in combination with a positive aero-propulsive balance with integration of high temperature resistant materials.
The complexity of the vehicle should be increased by integrating more subsystems while aiming for self-controlled operation. Meanwhile, larger projects should come around to gradually increase the vehicle size and hence reduce relatively the overall structural weight. This approach would bring the European transport industry globally in a strong competitive position.
Meanwhile, dedicated studies on hydrogen production and atmospheric emissions at high altitude should demonstrate the effectiveness of hydrogen as a fuel, if operated in a correct, economically viable way.

### The necessity and evidence of a European added value in HEXAFLY-INT

The *HEXAFLY-INT* project is an integration of the critical mass of partners, activities, expertise and resources across the full research spectrum necessary to achieve the accomplishment of high-speed commercial transport at flight Mach numbers of 4 to 8. The project will be exploiting existing and new knowledge across this critical mass:

1. *Not a single European country has the financial resources to support the comprehensive workprogramme* of *HEXAFLY-INT* because it is so know-how intensive and costly. Indeed, the breadth of facilities and expertise required, in high-speed airbreathing propulsion development, appropriate combustion technologies, and aerothermodynamic testing at high temperature and Mach numbers, is not available in any single laboratory, industry or country within Europe. *HEXAFLY-INT* builds on expertise gained from *ATLLAS I & II, LAPCAT-I & II*, *HEXAFLY and* previous in-house campaigns and national but also ESA funded research programs.

2. *HEXAFLY-INT will integrate contributions from internationally renowned European organisations across Europe*. These include leading research centres and all major engine manufacturers. This teaming of beneficiaries brings together the multidisciplinary mix of expertise that is required to deliver an integrated understanding of the advanced propulsion under investigation, and hence to indicate the major directions and to initiate the required technological building blocks, i.e. development, validation and exploitation of innovative propulsion concepts, and to release both scientific and economically beneficial deliverables. This approach will yield improved working practices and data consistency across the European research and industrial supply chain and reduce future product development lead times. The geographical spread of beneficiaries includes Italy, France, Germany, Belgium, the United Kingdom and the Netherlands.

3. *HEXAFLY-INT makes maximum use of international organisations worldwide*.
   Russia has unique aerodynamic and aero-propulsive facilities both in terms of size and test duration. This allows to ground-test a complete and flight-like vehicle mimicking a complete mission scenario with the related technologies prior to the flight. Making use of these facilities will ensure an important risk reduction for the actual flight.. Furthermore the connected tube facilities both in Russia allow an extensive and parallel investigation of multiple injector strategies in a comparative way prior to a final verification in the Russian free-jet facility and the actual flight. Further, to assure that the design of the flight vehicle doesn't deviate from the original passenger vehicle which needs to perform as well in the subsonic regime, the test range facility belonging to the University of Sydney is a welcome asset to evaluate the take-off and landing capabilities. Finally, the involved international partners involved are worldwide well known experts in the hypersonic community who are strongly motivated to work together on a unique international hypersonic project serving civil passenger transport.

#### 1.4.1.5 Potential areas and market of application

1. *System validation trough modelling and simulation*
   *HEXAFLY-INT* will contribute to achieve an increased predictive capability of CFD methods currently used by the Aeronautical industry. Advanced physical insight will lead to efficient modelling techniques for system studies, high-pressure and ram-based combustion and cooling techniques within the different parts of the engine. This achievement will contribute to an added value in advanced vehicle and propulsion design and therefore in increased modelling and simulation capabilities of the European industry and institutes.
2. *Decrease of noise emission*
   The *HEXAFLY-INT* proposal tackles explicitly the reduction of the sonic boom by looking into novel approaches to influence the parameters characterizing the pressure waveform (N-wave), i.e. the peak pressure, duration and rise time. The sonic boom intensity is proportional to square of the overpressure, so when the peak pressure decreases the sonic boom loudness reduces. The combination of low-loaded wings, blended wing-bodies and waveriders shall provide an alternative to sonic boom alleviation
3. *New shapes and sizes for aircraft*
   Supersonic aircrafts propelled by turbo- or ram-based air-breathing engines require a particular shape and size. This is intrinsically connected to a harmonized aircraft/engine integration in order to achieve an operational vehicle. All parts, intake, combustion chamber and nozzle do form an closed part of the complete aircraft. The forebody serves already as a part of the intake whereas the aftbody forms a part of the exit nozzle. This shape and size largely determine the optimal functioning of the engine and improve the total drag of the vehicle. This approach and methodology can be directly transferred to classical aircraft to increase their overall performance.

# 2 References


[1] Steelant J., "ATLLAS: Aero-Thermal Loaded Material Investigations for High-Speed Vehicles", *15th AIAA International Space Planes and Hypersonic Systems and Technologies Conference*, 28 April-1 May, 2008, Dayton, Ohio, USA, AIAA-2008-2582.

[2] Bouchez M., Dufour E., Le Naour B., Wilhelmi C., Bubenheim K., Kuhn M., Mainzer B., Riccius J., Davoine C. Justin J.-F., von Wolfersdorf J. Axtmann M., Villace F. and Steelant J., "Combustor Materials Research Studies for High Speed Aircraft in the European Program ATLLAS2", *20th International Space Planes and Hypersonic Systems and Technology Conference*, AIAA-2015-3639, 5-8 July 2015, Glasgow, UK.

[3] Steelant J., Dalenbring M. ., Kuhn M., Bouchez M. and von Wolfersdorf J., 'Achievements obtained within the ATLLAS-II Project on Aero-Thermal Loaded Material Investigations for High-Speed Vehicles', 21st Int. Space Planes and Hypersonic Systems and Technology Conference, AIAA-2017-2393, 6-9 March 2017, Xiamen, China.

[4] Steelant J., 'Achievements Obtained for Sustained Hypersonic Flight within the LAPCAT Project', 15th AIAA International Space Planes and Hypersonic Systems and Technologies Conference, AIAA-2008-2578, 28 April- 01 May 2008, Dayton, Ohio, USA.

[5] Steelant, J., Varvill, R., Defoort, S., Hannemann, K., and Marini, M., "Achievements Obtained for Sustained Hypersonic Flight within the LAPCAT-II project", *20th AIAA International Space Planes and Hypersonic Systems and Technologies Conference*, Glasgow, Scotland, July 6-9, 2015: AIAA-2015-3677.

[6] Pezzella, G., Marini, M., Cicala, M., Vitale, A., Langener, T., Steelant, J., "Aerodynamic Characterization of HEXAFLY Scramjet Propelled Hypersonic Vehicle", *32nd AIAA Aviation (Applied Aerodynamics Conference)*, 16-20 June 2014, Atlanta, GA: AIAA 2014-2844.

[7] Steelant, J., Langener, T., Di Matteo, F., Hannemann, K., Riehmer, J., Kuhn, M., Dittert, C., Scheuerpflug, F., Jung, W., Marini, M., Pezzella, G., Cicala, M., Serre, L., "Conceptual Design of the High-Speed Propelled Experimental Flight Test Vehicle HEXAFLY", *20th AIAA International Space Planes and Hypersonic Systems and Technologies Conference*, Glasgow, Scotland, 6-9 July 2015: AIAA-2015-3539.

[8] Roberto Scigliano , Giuseppe Pezzella, Sara Di Benedetto, Marco Marini, Johan Steelant, "HEXAFLY-INT Experimental Flight Test Vehicle (EFTV) Aero-Thermal Design", ASME International Mechanical Engineering Congress & Exposition (IMECE), IMECE2017-70392, 3-9 November 2017, Tampa, Floride, USA.

[9] Roberto Scigliano, Valerio Carandente, Design Analysis Of The Hexafly-Int Thermal Protection System, 8th European Workshop on TPS & Hot Structures, 19-22 April 2016, ESA/ESTEC, Noordwijk, The Netherlands.

[10] Favaloro, N., Rispoli, A., Vecchione, L., Pezzella, G., Carandente, V., Scigliano, R., Cicala, M., Morani, M., Steelant, J., "Design Analysis of the High-Speed Experimental Flight Test Vehicle HEXAFLY-International", *20th AIAA International Space Planes and Hypersonic Systems and Technologies Conference*, Glasgow, Scotland, 6-9 July 2015: AIAA-2015-3607.

[11] Pezzella, G., Marini, M., Reimann, B., Steelant, J., "Aerodynamic Design Analysis of the Hexafly-INT Hypersonic Glider", *20th AIAA International Space Planes and Hypersonic Systems and Technologies Conference,* Glasgow, Scotland, 6-9 July 2015: AIAA-2015-3644.

[12] Schettino A., Pezzella G., Marini M., Di Benedetto S., Villace V. F., Steelant J., Gubanov A. and Voevodenko N., 'Aerodynamic and Aerothermodynamic Database of the HEXAFLY-INT Hypersonic Glider', International Conference on High-Speed Vehicle Science and Technology (HiSST), 26-29/11/2018, Moscow, Russia, HiSTT-2018-2940957.

[13] Steelant J., Passaro A., Fernandez-Villace V., Gubanov A.A., Ivanyushkin D.S., Shvalev Yu.G., Voevodenko N.V., Marini M., Di Benedetto S. 'Boundary layer transition assessment on a slender high-speed vehicle', 21st Int. Space Planes and Hypersonic Systems and Technology Conference, AIAA-2017-2133, 6-9 March 2017, Xiamen, China.

[14] Pezzella, G., Carandente, V., Scigliano, R., Marini, M., Steelant, J., "Aerothermal Environment Methodology of the Hexafly-Int Experimental Flight Test Vehicle (EFTV)". *8th European Symposium on Aerothermodynamics for Space Vehicles*. 2-6 March 2015. Lisbon. Portugal. European Space Agency.

[15] Carandente, V., Scigliano, R., Pezzella, G., Marini, M., and Steelant, J., "Finite Element Thermal Design of the Hexafly-INT Experimental Flight Test Vehicle". *6th European Conference for Aeronautics and Space Sciences (Eucass)*. 29 June-3 July, 2015, Krakow, Poland.

[16] Steelant J. and Langener T., "The LAPCAT-MR2 Hypersonic Cruiser Concept", ICAS-2014-0428, *29th Congress of the International Council of the Aeronautical Sciences*, St. Petersburg, Russia, September 7-12, 2014.
[17] Kennell C., Neely A., O'Byrne S, Buttsworth D., 'Measurement of Vehicle Stability Coefficients in Hypersonic Wind Tunnels', *20th AIAA International Space Planes and Hypersonic Systems and Technologies Conference*, Glasgow, Scotland, 6-9 July 2015: AIAA-2015-3690.
[18] Kennell C., Neely A., Tahtali M., Buttsworth D.R., Choudhury R., "Free Flight Testing in Hypersonic Flows: HEXAFLY-INT EFTV", *AIAA SciTech*, AIAA 2016-1088.
[19] Buttsworth D.R., "Ludwieg Tunnel Facility with Free Piston Compression Heating for Supersonic and Hypersonic Testing", *9th Australian Space Science Conference 2009*, Published 2010.
[20] Nebula F., Morani G., Mattei G., Di Donato M.P., Rispoli A., Menchetti C. and Steelant J., 'Selection and Performance Evaluation of the Navigation unit for the HEXAFLY-INT Hypersonic Mission', 1st International Conference on High-Speed Vehicle Science and Technology (HiSST), 26-29/11/2018, Moscow, Russia.
[21] Di Benedetto S., Di Donato M. P., Rispoli A., Pezzella G., Scigliano R., Nebula F., Cristillo D., Cardone S., Steelant J., Villace V. and Vecchione L., 'Multidisciplinary Design and Flight Test of the HEXAFLY-INT Experimental Flight Vehicle', 1st International Conference on High-Speed Vehicle Science and Technology (HiSST), 26-29/11/2018, Moscow, Russia.
[22] Andro J.-Y., Scigliano R., Kallenbach A. and Steelant J., 'Thermal Management of the Hexafly-Int Hypersonic Glider', 1st International Conference on High-Speed Vehicle Science and Technology (HiSST), 26-29/11/2018, Moscow, Russia.
[23] Andro J.-Y., Rotärmel W., Nebula F., Morani G., and Steelant J., 'Design of the Actuation System of the Hexafly-Int Hypersonic Glider', 1st International Conference on High-Speed Vehicle Science and Technology (HiSST), 26-29/11/2018, Moscow, Russia.
[24] Munk D. J., Vio G. A. , Verstraete D. and Steelant J., 'Structural Topology Optimisation of the HEXAFLY-INT Vertical Fin', 1st International Conference on High-Speed Vehicle Science and Technology (HiSST), 26-29/11/2018, Moscow, Russia.
[25] Bykerk T., Verstraete D., Wolf S., Villace V. and Steelant J., 'Performance and Stability Analysis of a Hypersonic Vehicle for a Low Speed Flight Test Program', 1st International Conference on High-Speed Vehicle Science and Technology (HiSST), 26-29/11/2018, Moscow, Russia.
[26] Choudhury R., Villace V. F. , Steelant J. and Buttsworth D., 'Micro-Aerothermodynamic Analysis of Protuberances on a Hypersonic Glider Using a Reduced Domain Approach', 1st International Conference on High-Speed Vehicle Science and Technology (HiSST), 26-29/11/2018, Moscow, Russia.
[27] M. A. Ivankin, A. A. Nikolaev, V. A. Talyzin and O. V. Voloschenko, 'Investigation of the Hydrogen Combustion Chamber Performance within the International HEXAFLY-INT Project', 30th Congress of the International Council of the Aeronautical Sciences (ICAS-2016), ICAS2016_458, Daejeon, Korea, 25th – 30th September, 2016
[28] Aleksandrov V.Yu., Kukshinov N.V., Prokhorov A.N., Rudinskiy A.V. Analysis of the integral characteristics of HEXAFLY-INT facility module. *21st AIAA International Space Planes and Hypersonic Systems and Technologies Conference*. Xiamen, China, March 6-9, 2017: AIAA-2017-2179.
[29] Aleksandrov V.Yu., Danilov M.K., Gouskov O.V., Gusev S.V., Kukshinov N.V., Prokhorov A.N., Zakharov V.S. Numerical and experimental investigation of different intake configurations of HEXAFLY-INT facility module. *30th Congress of the International Council of the Aeronautical Sciences (ICAS)*. Daegeon, Korea, September 26-30, 2016: ICAS-2016-0380.
[30] Aleksandrov V.Yu., Batura S.N., Gouskov O.V., Kukshinov N.V., Prokhorov A.N., Rudinskiy A.V. Complex numerical and experimental research of HEXAFLY-INT high-speed civil aircraft. *31th Congress of the International Council of the Aeronautical Sciences (ICAS)*. Belo Horizonte, Brazil, September 09-14, 2018: ICAS-2018-0672.
[31] Gubanov A.A., Ivanyushkin D.S., Kukshinov N.V., Prokhorov A.N., Talyzin V.A., Voevodenko N.V. Investigation on aero-propulsive balance for high-speed powered experimental flight test vehicle within the HEXAFLY-INT project. *31th Congress of the International Council of the Aeronautical Sciences (ICAS)*. Belo Horizonte, Brazil, September 09-14, 2018: ICAS-2018-0508.